Druglike, ^{18}F-labeled PET tracers targeting fibroblast activation protein (FAP)

Druglike, ^{18}F-labeled PET tracers targeting fibroblast activation protein (FAP)

Muhammet Tanc[†], Nicolò Filippi[†], Yentl Van Rymenant[‡], Sergei Grintsevich[†], Isabel Pintelon[ʃ], Marlies Verschuuren[ʃ], Joni De Loose[‡], Emile Verhulst[‡], Euy Sung Moon[≠], Lorenzo Cianni[†], Sigrid Stroobants[#], Koen Augustyns[†], Frank Roesch[≠], Ingrid De Meester[‡], Filipe Elvas[#,‖,], Pieter Van der Veken,[†,‖,*]*

[†]Laboratory of Medicinal Chemistry, Department of Pharmaceutical Sciences, University of Antwerp, Universiteitsplein 1, 2610 Wilrijk, Belgium

[‡]Laboratory of Medical Biochemistry, Department of Pharmaceutical Sciences, University of Antwerp, Universiteitsplein 1, 2610 Wilrijk, Belgium

[ʃ]Laboratory of Cell Biology and Histology, Department of Veterinary Sciences, University of Antwerp, Universiteitsplein 1, 2610 Wilrijk, Belgium

[≠]Institut für Kernchemie, Johannes Gutenberg University of Mainz, Fritz-Strassman-Weg 2, D-55128 Mainz, Germany

[#]Molecular Imaging and Radiology, Faculty of Medicine and Health Sciences, University of Antwerp, Universiteitsplein 1, 2610 Wilrijk, Belgium

[‖]These authors contributed equally

* Corresponding authors

Current address Muhammet Tanc: Division of Imaging Sciences and Biomedical Engineering, King's College, London, UK

Keywords: fibroblast activation protein, FAP, druglike PET tracers, ^{18}F

ABSTRACT

Fibroblast activation protein (FAP) is a very reliable biomarker for tissue remodeling. FAP has so far mainly been studied in oncology, but there is growing interest for the enzyme in other diseases like fibrosis. Recently FAP-targeting diagnostics and therapeutics have emerged, of which the so-called FAPIs are among the most promising representatives. FAPIs typically have a relatively high molecular weight and contain very polar, multi-charged chelator moieties. While this is not limiting the application of FAPIs in oncology, more druglike FAPIs could be required to optimally study diseases characterized by denser, less permeable tissue. In response, we designed the first druglike ^{18}F-labeled FAPIs. We report target potencies, biodistribution and pharmacokinetics and demonstrate FAP-dependent uptake in murine tumor xenografts. Finally, this paper puts forward compound **10** as a highly promising, druglike FAPI for ^{18}F-PET imaging. This molecule is fit for additional studies in fibrosis and its preclinical profile warrants clinical investigation.

INTRODUCTION

Fibroblast activation protein (FAP) is a cell surface marker of activated fibroblasts associated with tissue remodeling processes. FAP is abundantly expressed on *cancer-associated-fibroblasts* (CAFs) in the micro-environment of nearly all tumor types. Likewise, FAP-positive fibroblasts are also present in lesions associated with chronic inflammatory disorders, including fibrotic processes, arthritis and atherosclerosis.[1-5] Noteworthy, FAP is negligibly expressed in healthy adult tissues.[2-4] Functionally, FAP is a proline-selective serine protease that is closely related to the well-known dipeptidyl-peptidases (DPPs). Intense research is currently ongoing to characterize the enzyme's multiple functions in tissue remodeling: these

range from extracellular matrix (ECM) remodeling to local immune response regulation. The detailed functional characterization, however, is far from complete.[1]

In oncology, most attention currently goes to using FAP as a tumoral anchor point for cancer diagnostics and therapeutics. The status of FAP as a pan-cancer biomarker suggests nearly universal applicability of diagnostic FAP-targeting in this domain. Accordingly, FAP-targeted positron emission tomography (PET) imaging has emerged as a new approach for noninvasive and quantitative imaging of cancer. Tapping this exceptional potential has originally been pursued with radiolabeled monoclonal FAP-antibodies (mAbs). This effort, however, never materialized into EMA/FDA approved products.[6] In 2014, our research group has reported UAMC1110 (compound **1**, **Figure 1**): to date still the most potent and selective small molecule inhibitor of FAP.[7,8] UAMC1110 has since then been used as the basis for most so-called FAPIs: a new generation of tumor-targeting constructs that bind to FAP.[9,10] A typical FAPI consists of 1) a UAMC1110 moiety for tumor targeting and 2) a diagnostic or a therapeutic payload, *e.g.*, a radionuclide (**Figure 1**). In most reported molecules, the latter is a radiometal, kept in place by a chelator and attached to UAMC1110 via a linker moiety.

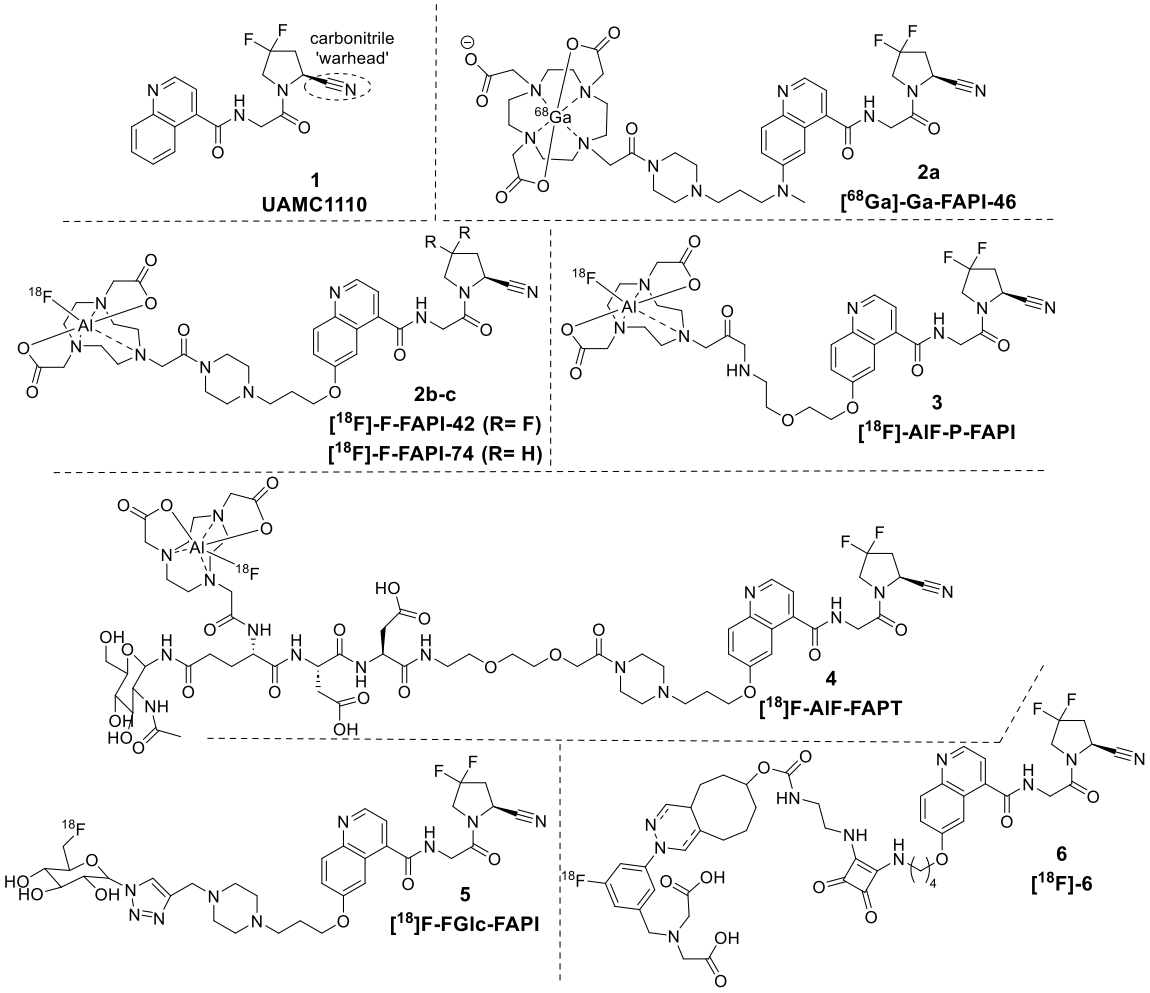

Figure 1. UAMC1110 (compound **1**) and relevant examples of UAMC1110-derived FAPIs.

Several of these FAPIs are being investigated clinically for PET-oncodiagnostics applications in a wide variety of cancer types. Particularly convincing results have been reported for the FAPI-series developed by Haberkorn and colleagues. Compounds like FAPI-04, or FAPI-74 have demonstrated improved imaging quality of patients suffering from many tumors, in particular in cases where tumors are not readily detectable with fluorine-18-labeled fluorodeoxy glucose ([^{18}F]FDG), which is the current reference standard for cancer imaging.[11] Within the FAPI-diagnostics field, most attention initially went to ^{68}Ga-labeled compounds, but research towards ^{18}F-labeled FAPIs is currently also receiving a lot of attention. Next to the superior spatial resolution that can theoretically be obtained with ^{18}F-PET imaging, the relatively longer

half-life of ^{18}F ($t_{1/2}$ = 109.8 min, compared to $t_{1/2}(^{68}Ga)$= 67.7 min), makes ^{18}F more practical to work with. Related to this, availability of ^{68}Ga is limited by the fact that it needs to be produced on-site in relatively small batches, by means of a $^{68}Ge/^{68}Ga$-generator. Conversely, ^{18}F can be produced in large batches in a cyclotron and can also be transported to satellite PET-centers that lack radionuclide production capabilities.[12] Again, representatives of the original FAPIs (compounds **2a-c**) reported by Haberkorn appear to be the most advanced. Relevant examples of ^{18}F-labeled representatives, include [^{18}F]AlF-FAPI-42 and [^{18}F]AlF-FAPI-74 (compounds **2b-c**, **Figure 1**).[12,13] In these, the ^{18}F-label is coordinated to an aluminum fluoride complex, which itself is fixed inside a NOTA-ligand. Comparable analogs with modified linkers have been published by others, for example compounds **3** ([^{18}F]AlF-P-FAPI) and **4** ([^{18}F]AlF-FAPT) that were reported by Tang et al. and Huang et al.[14,15] Overall, preclinical evaluations of these compounds shows satisfactory and selective tumor uptake. Of note, hepatobiliary excretion seems to be a drawback of most reported ^{18}F-labeled compounds, except in cases where lipophilicity of the tracers is decreased. This, for example, is illustrated by the predominant renal excretion pattern observed for [^{18}F]AlF-FAPI-74, a compound that lacks the difluoro-substituents on the pyrrolidine ring. In humans, nonetheless, hepatobiliary excretion seems to be a less prominent feature based on the limited data that are available for, e.g., compound **3**.[12,13]

Of note, however, the large chelator/radiometal moieties in all these molecules discount on the druglikeness of these compounds, as they strongly increase parameters like molecular weight, polar surface area and number of hydrogen bond donors/acceptors. This can be a limiting factor for the membrane and tissue permeability of these molecules. Druglikeness ca be expected not to be a critical parameter for oncology applications of FAPIs, because tumors are characterized by leaky vasculature and, generally, loose tissue. This allows FAPIs to

relatively easily enter and diffuse through tumoral tissue. In other, very dense tissue types (as, *e.g.*, in fibrosis), druglikeness might however become an important parameter. The ongoing preclinical and clinical evaluation of the FAPIs as PET diagnostics for fibrosis will most likely shed more light on this important prerequisite for FAPIs.[16,17]

In addition, a limited number of ^{18}F-labeled tracers have been described in which the fluorine atom is covalently linked to the FAPI. A representative example is compound **5** that was reported by Toms and co-workers (**Figure 1**).[18] Another very recent example is tracer **6** (also shown in **Figure 1**), which was reported as '**[^{18}F]-6**' by Poulie and co-workers.[19] In this compound, the ^{18}F-radiolabel was introduced via tetrazine-*trans*-cyclooctene ligation. In spite of good and specific tumor uptake, none of these compounds can be really envisaged as druglike, and none of them performs better than the leading chelator-based references, for example with respect to tumor uptake and background signals. With this background, we started conceiving more druglike ^{18}F-labeled FAPIs in which the ^{18}F-label is covalently attached to the UAMC 1110 moiety via a very short linker. Similar to the findings of Haberkorn et al., our first attempts with molecules of this kind also indicated that the polarity and nature of the linker moiety are crucial for *in vivo* compound stability and determine the excretion pathway (hitherto unreported data).[12,13] Therefore, we hypothesized that molecules in which one or two polar groups decorate the short linker moiety would have more desirable *in vivo* behaviour. Taking into account that introducing too much polarity in the linker could also jeopardize tissue permeability, the following small, polar group types were selected: 1) the methoxy substituent in compound **7,** 2) the alcohol and vicinal diol groups in compounds **8** and **9**, and 3) the quaternary ammonium group in compound **10** (**Figure 2**). A quaternary ammonium group was preferred over a classical, basic amine group for several reasons. First, the positive charge in **10** is relatively more shielded than in an analogous protonated amine.

In addition, the *N*-methylsubstituents are also inductive donors, that slightly compensate the positive charge and in this way further reduce polarity compared to an amine group.

While the radiolabeling of **7**, **8** and **9** can be performed via conventional nucleophilic substitution with [^{18}F]fluoride, a somewhat more elaborate [^{18}F]fluoroalkylation strategy is required for radiolabeling **10**. Of note, we chose to introduce a fluoro-(di-deutero)methyl over the classical fluoromethyl substituent, because the former has been reported to be more stable *in vivo*.[20]

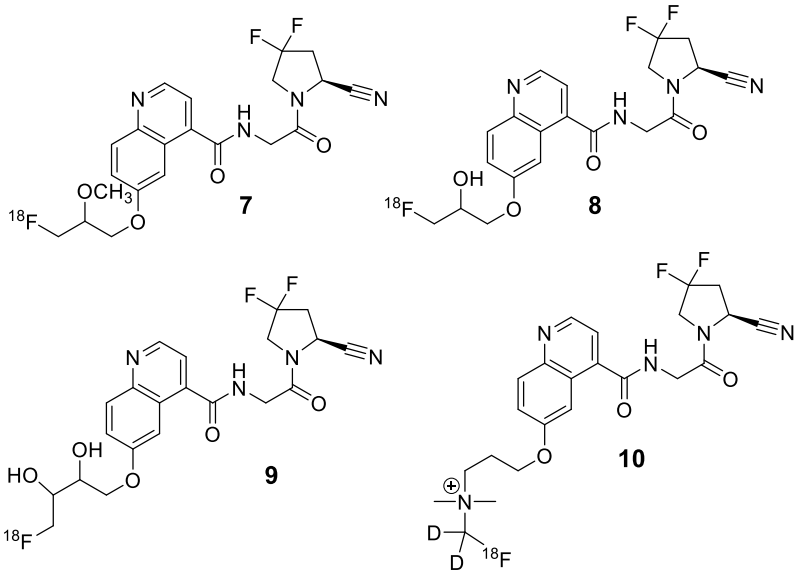

Figure 2. Target compounds of this study: druglike, ^{18}F-labeled PET probes.

We decided to study these compounds first in preclinical, *in vivo* oncology settings. This is because murine models in this domain are currently best characterized for FAP-expression and because these models currently are the literature standard for new FAPI derivatives. This allows straightforward comparison between these and other reported compounds.

CHEMISTRY

First, the radiosynthesis precursors for target compounds **7**-**10** were prepared, along with the corresponding 'cold' (*i.e.*, ^{19}F-containing) references (**Schemes 1-3**). For the methoxy- and hydroxy substituted **7** and **8**, intermediates **14** and **16** were first prepared separately (**Scheme 1**). The 1,3-dibenzyl derivative of glycerol **11** was prepared via the published procedure of Nemeto and co-workers.[21] Methylation of the 2-hydroxy group, followed by hydrogenative de-benzylation delivered **13**. The latter was *bis*-tosylated with tosyl chloride to obtain **14.** In parallel, 1,3-*bis*-tosylated glycerol **15** was prepared via the method of Oh and co-workers.[22] Reaction with dihydropyrane in acidic conditions yielded the tetrahydropyranyl (THP)-protected building block **16**. Both **14** and **16** were used separately to alkylate the phenol group of **17**, rendering intermediates **18a-b**, while selective saponification of these molecules' methyl ester groups resulted in **19a-b**. Coupling of the two latter intermediates with glycyl-(2-cyano-4,4-difluoropyrrolidine), prepared via the published method of Tanc et al., gave the radiosynthesis precurors **20** and **21.**[23] The tosylate group in these compounds was intended to be nucleophilically substituted with [^{18}F]F$^-$ during the radiofluorination (*vide infra*). In addition, nucleophilic substitution with ^{19}F$^-$ was also carried out by reaction of TBAF with the tosylated intermediates **19a-b**, delivering the corresponding **22a-b**. Coupling with HATU of the latter to glycyl-(2-cyano-4,4-difluoropyrrolidine) yielded the 'cold' references **23** and **24**, either directly or after acidic hydrolytic cleavage of the THP-protecting group. Finally, it deserves mentioning that the alkylation reaction of **17** installs a stereocenter at the 2-position of the prochiral, glycerol derived linker. The resulting intermediate **18** can reasonably be anticipated to occur as a racemate. Final products, however, also contain a second stereocenter at the 2-position of the pyrrolidine ring. Since this moiety is derived from natural L-proline, it has a fixed *S*-configuration. This implies that final products in **Scheme 1** are obtained as a 1:1

mixture of 2 diastereomers. Since these 2 diastereomers behave identically in all chromatographic separations tried, all downstream experiments were carried out with this mixture of diastereomers.

Scheme 1. Synthesis of radiosynthesis precursors and cold references for PET-tracers **6** and **7**.

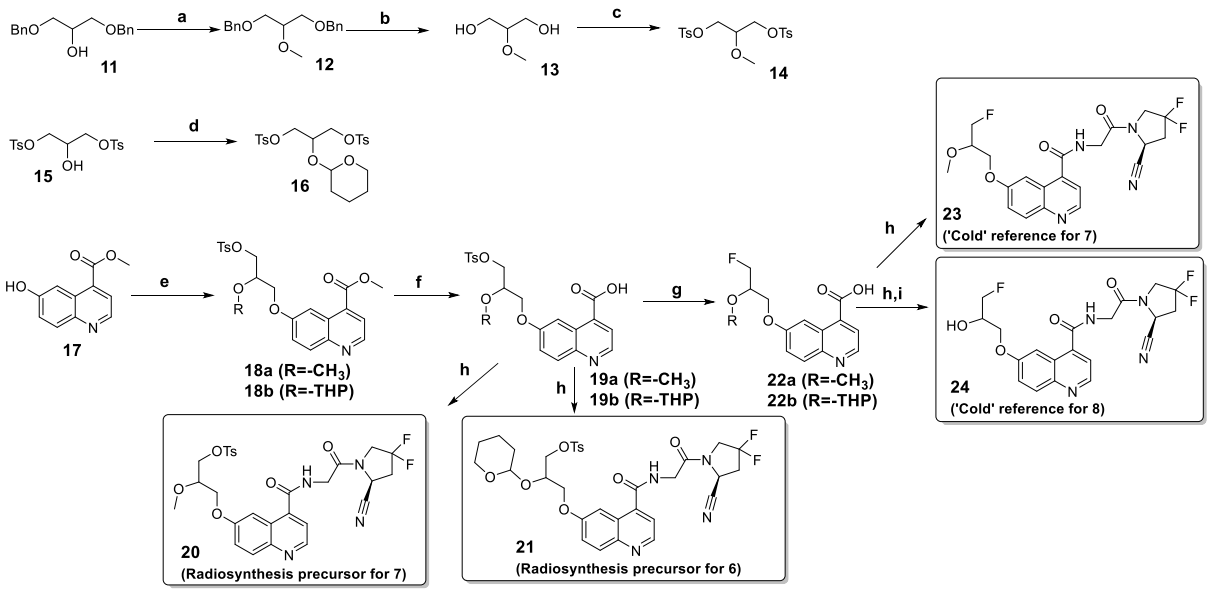

Reagents and conditions. (a) NaH (1.1 eq.) , MeI (1.2 eq.), dry DMF, 0 °C – rt, 2 h, 72%; (b) $Pd(OH)_2$ (1 mol%), H_2, MeOH, rt, 12 h, quant.; (c) TosCl (2.1 eq.), pyridine (4 eq.) CH_2Cl_2, rt, 2 h, 59%; (d) dihydropyran (4 eq.), pyridinium tosylate (4 eq.), dry CH_2Cl_2, 40°C, 2 h, 89%; (e) ***14*** *(1.2 eq) or* ***16*** *(1.2 eq.), Cs_2CO_3 (5 eq.), dry DMF, rt - 40 °C , 5 h, 52%; (f) NaOH (5 eq.) MeOH, 40 °C, 2 h, 71%; (g) TBAF (5 eq.), ACN, 80°C, 24 h, 16%; (h) glycyl-(2-cyano-4,4-difluoropyrrolidine), HATU (1.1 eq.), DIPEA (5 eq.), DMF, rt, 18-90%; (i) pyridinium tosylate (4 eq.), H_2O (4 eq.), THF, 40 °C, 2 h, 90-95%*

An overall comparable strategy was followed for the synthesis of the common radiosynthetic precursor of **9** and the 'cold' references of these compounds. (**Scheme 2**). More precisely, the phenolic -OH group of **17**, was alkylated with commercially available, *bis*-tosylated

butanetetrol derivative **25**. Since the commercial **25** consists entirely of the achiral *trans*-isomer, alkylation is again expected to yield 2 enantiomeric forms of **26** in a 1:1 ratio. These 2 enantiomers both have a *trans*-configuration in the acetonide ring. They were not separated but were directly subjected to selective saponification of their methyl ester, yielding racemic **27.** The latter was coupled to glycyl-(2-cyano-4,4-difluoropyrrolidine) using HATU to obtain the tosylated precursor **28**. Alternatively, the tosyl group in **27** was subjected to nucleophilic substitution with fluoride ion, and the resulting **29** was subsequently coupled to glycyl-(2-cyano-4,4-difluoropyrrolidine) to obtain **30**. Applying acidic hydrolysis conditions to **30** was instrumental for removing the acetonide protecting group to obtain 'cold' reference **31**. Based on the same stereochemistry considerations that were described for **Scheme 1** (*vide supra*) all final products from **Scheme 2** were obtained as a mixture of 2 diastereomers in a 1:1 ratio. Since these molecules were inseparable in the chromatographic systems evaluated, they were evaluated together in downstream experiments.

Scheme 2: Synthesis of radiosynthesis precursors and cold references for PET-tracers **8** and **9**.

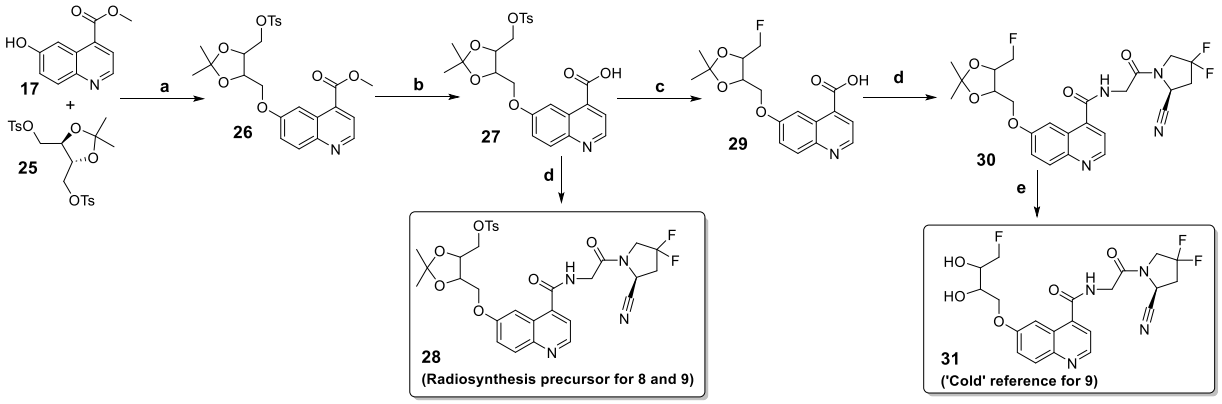

Reagents and conditions. (a) 2,2-dimethyl-1,3-dioxolane-4,5-diyl)bis(methylene) bis(4-methylbenzenesulfonate (1.2 eq) Cs_2CO_3 (4 eq.), dry DMF 40 °C 20 h, 31%; (b) NaOH (5 eq.), dry MeOH, rt, 8 h, quant.; (c) TBAF (5 eq.), ACN, 80°C, 24 h, 16%; (d) glycyl(2-cyano-4,4-difluoropyrrolidine), *HATU (1.1 eq.), DIPEA (5 eq.), DMF, rt, 16-69% (e) pyridinium tosylate (4 eq.), H_2O (4 eq.), THF, 40°C, 2 h, 90-95%.*

Finally, the radiosynthesis precursor and 'cold' reference for compound **10** involved the preparation of the chloropropoxy-substituted quinoline derivative **32**, according to a procedure published by Lindner et al.[9] (**Scheme 3**) This compound was submitted to aliphatic nucleophilic substitution with dimethylamine. The obtained **33** was subsequently coupled with HATU to render radiosynthesis precursor **34**. Fluoromethylation of the latter with *O*-fluoromethyl tosylate, rendered cold reference **35**.[24] Because **35** was not intended for *in vivo* evaluation, synthesis of the di-deutero analogue was deemed not to be required.

Scheme 3: Synthesis of radiosynthesis precursors and cold references for PET-tracers **10**.

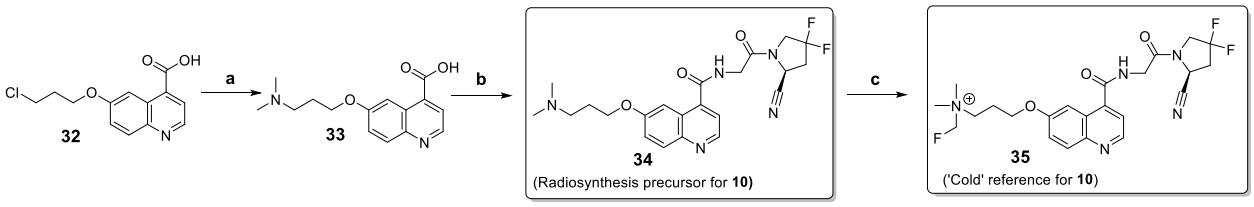

Reagents and conditions. (a) Dimethylamine (4 eq.), KI (4 eq.), dry DMF 60 °C, 16 h, 45%; (b) glycyl-(2-cyano-4,4-difluoropyrrolidine), HATU (1.1 eq.), DIPEA (5 eq.), DMF, rt, 48%; (c) Fluoromethyl-4-methylbenzenesulfonate (5 eq.), DIPEA (5 eq.), DMF, 120 °C, 20 min, 10%.

BIOCHEMICAL EVALUATION

The cold references **23**, **24**, **31** and **35** were first investigated for FAP-affinity and also for selectivity with respect to the other proline-selective proteases: the dipeptidyl-peptidases (DPPs) and the endopeptidase prolyl oligopeptidase (PREP). Since the DPPs and PREP are ubiquitously expressed in the human body, it is important to evaluate the selectivity and affinity of the FAP ligands before performing subsequent *in vivo* experiments.[7,8] Results are summarized in **Table 1**. FAP-potency and selectivity were also determined for the acetonide-protected compound **30**: because acetal functionalities can be metabolically instable, it was anticipated that **30** could potentially find later application as a prodrug for the diol-containing **31**.[25] In addition, affinity and selectivity data are provided for several general reference compounds: **1**, **36** and **37**. (**Figures 1 and 3**) Compound **1** is UAMC1110, the parent FAP-inhibitor of most FAPIs, while **36** and **37** are two are well-known literature standards that, after labeling with ^{68}Ga, were used as references in the PET-imaging study (*vide infra*).

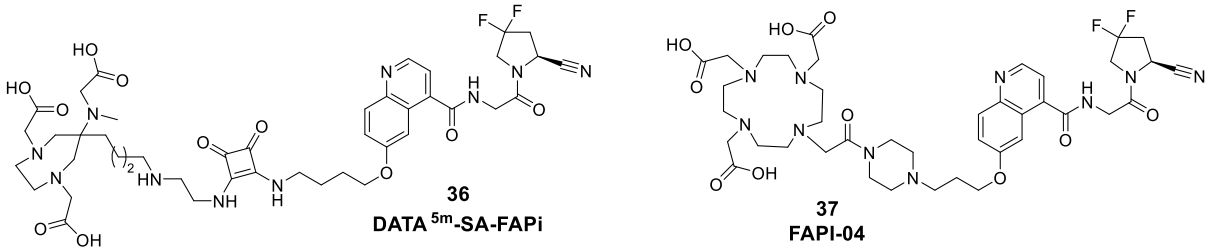

Figure 3. General reference molecules DATA^{5m}-SA-FAPi (**36**) and FAPI-04 (**37**).

Table 1. IC_{50} values for 'cold' references (**23, 24, 30, 31 and 35**) and literature references used in this study (**1**, **36** and **37**).

Cmpd.	**IC_{50} (nM)[(a)]**	**IC_{50} (µM)**				
	FAP	**DPP4**	**DPP8**	**DPP9**	**DPP2**	**PREP**
1	0.43 ± 0.02	> 10	4.7 ± 0.4	> 10	> 10	1.8 ± 0.01
23	1.4 ± 0.1	> 10	5.8 ± 0.3	1.6 ±0.4	> 10	> 10
24	4.37 ± 0.17	> 10	> 10	> 10	> 10	> 10
30	0.46 ± 0.02	> 10	> 10	> 10	> 10	> 10
31	1.77 ± 0.08	> 10	> 10	> 10	> 10	> 10
35	0.32 ± 0.02	> 10	> 10	> 10	> 10	> 10
36	0.8 ± 0.2	n.d.	n.d.	n.d.	n.d.	1.7 ± 0.1
37	0.21 ± 0.02	n.d.	n.d.	n.d.	n.d.	8.4 ± 1.6

[(a)] Data are presented as mean with standard deviation (n = 3).

Overall, the FAP-potencies of all new compounds are in the low nanomolar range (0.32 – 4.37 nM), whereas the IC_{50} values for PREP and the DPPs are in the micromolar range. This potency and selectivity profile justifies further preclinical examination of the new compounds as PET-

probes: all molecules were therefore progressed to radiosynthesis and characterization of key biopharmaceutical parameters.

RADIOCHEMISTRY AND STABILITY EVALUATION

Radiofluorination of precursors **20**, **21**, **28, 34** was performed using an automated radiosynthesis module, yielding the corresponding radioligands [^{18}F]**7**, [^{18}F]**8**, [^{18}F]**9** and [^{18}F]**10**. Optimized reaction conditions for each of the tracers are shown in **Scheme 4**. The tosylated precursors **20**, **21** and **28**, were subjected to nucleophilic substitution with ^{18}F-fluoride ion, which in the case of the THP-and acetonide-protected precursors **21** and **28** was followed by acidic hydrolysis of the protecting groups. For synthesis of the quaternary ammonium-based **10**, [^{18}F]fluoromethyl bromide-d_2 (**38**) was first prepared in one step by reacting dibromomethane-d_2 with [^{18}F]fluoride via nucleophilic substitution. Subsequently, tertiary amine precursor **34** was quaternized with [^{18}F]**38**. This approach in our hands gave better results over other literature methods for preparation [^{18}F]fluoro-[di-deutero]methylation.[20,24] Finally, the reference radioligands **36** and **37** were radiolabeled with ^{68}Ga following literature procedures (not shown in **Scheme 4**).[9,26]

Scheme 4: Radiosynthetic procedures for the preparation of 7, 8, 9 and 10.

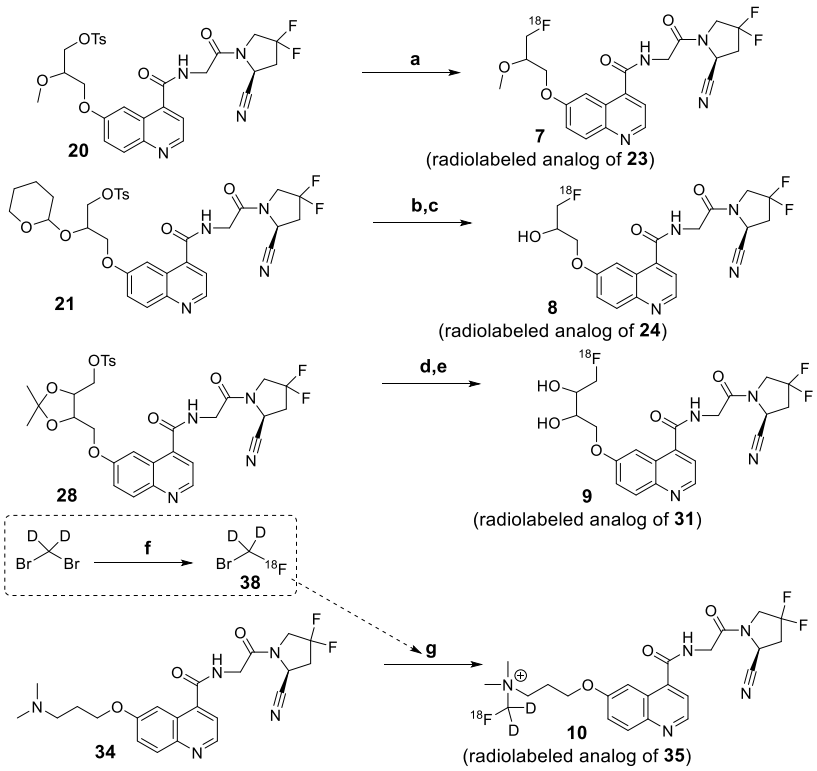

Reagents and conditions. (a) [^{18}F]fluoride, tetraethylammonium bicarbonate (TEAB), DMSO, 105°C, 10 min; (b) [^{18}F]fluoride, TEAB, DMSO, 110°C, 10 min; (c) 4N HCl in dioxane, 40°C, 2 min; (d) [^{18}F]fluoride, TEAB, DMSO, 110°C, 9 min; (e) 4N HCl in dioxane, 40°C, 3 min; (f) [^{18}F]fluoride, K_2CO_3/Kryptofix 222, ACN, 90°C, 5 min; (g) ***38****, DMF, 100°C, 10 min.*

All radiofluorinated compounds were obtained in moderate radiochemical yield (RCY), high radiochemical purity (RCP) and good molar activity (A_m). (data summarized in **Table 2**) The ^{68}Ga-labeled references, [^{68}Ga]Ga-DATA^{5m}.SA.FAPi (**36**, n=4) and [^{68}Ga]Ga-DOTA-FAPI-04 (**37**, n=2) were successfully labeled as previously described.[9,26] The isolated radiochemical yields were > 95% and > 85% (decay corrected), and the apparent molar activities (A_m) were 19.7 ± 0.5 (n=4) and 8.9 ± 0.4 GBq/µmol (n=2), respectively.

The radiosynthesis module is routinely used in a clean room environment and can facilitate the clinical translation of the developed PET radioligands. The identity of the radiolabeled

compounds was confirmed by co-injection and co-elution on HPLC of each radiofluorinated tracer with the corresponding 'cold' reference compounds (Shown in Supporting Information).

Table 2: FAP radioligand characterization.

Cmpd.	Radiochemical Yield (%) (decay-corrected) [(a),(b)]	Molar Activity (GBq/µmol)[(a),(b)]	Radiochemical Purity (%)[(b)]	LogD[(b)]
[^{18}F]**7**	3.6 ± 1.2	49.8 ± 13.2	99.8 ± 0.2	0.77 ± 0.02
[^{18}F]**8**	3.5 ± 1.3	46.7 ± 18.6	98.2 ± 0.3	0.18 ± 0.01
[^{18}F]**9**	2.6 ± 0.9	43.8 ± 10.9	97.5 ± 1.7	-0.27 ± 0.01
[^{18}F]**10**	5.8 ± 1.2	240.3 ± 171.3	99.2 ± 1.1	-1.77 ± 0.01

[(a)] Measured at end of bombardment.
[(b)] Data are presented as means of n independent experiments with standard deviation, Cmpd **7**: n=4; Cmpd. **8**: n=3; Cmpd. **9**: n=4; Cmpd. **10**: n=8.
.

For all radiolabeled compounds, LogD-values were determined: these are also shown in **Table 2**. Out of all ^{18}F-labeled FAP ligands, the quaternary ammonium-containing **10** was found to be the most hydrophilic (LogD= -1.77 ± 0.01). As expected, however, this is still significantly less hydrophilic than [^{68}Ga]**36** (LogD=-3.58 ± 0.04) and [^{68}Ga]**37** (-3.46 ± 0.04), that contain a very polar, poly-charged chelator moiety. This is supportive of the hypothesis that the smaller and more lipophilic quaternary ammonium-based **10**, could have a better tissue permeability than the chelator-based molecules. Finally, before initiating the *in vivo* studies, the stability of all 4 novel radioligands was also determined in PBS and mouse plasma. As shown in **Figure 4**, all radioligands showed excellent *in vitro* stability in PBS and mouse plasma at 37°C up to 60 min, with most of the parent radiotracers (intact tracer > 70%) being detected by radio-HPLC, without signs of major degradation. The stability of [^{18}F]**7**, [^{18}F]**8**, [^{18}F]**9** and [^{18}F]**10** was subsequently evaluated *in vivo* at different time points following intravenous (*i.v.*) injection of

the radiotracers in nude mice (**Figure 4**). Radio-HPLC analysis of the plasma revealed very good *in vivo* stability for [^{18}F]**10** (56.5 ± 7.8% intact at 60 min post-radioligand injection), whereas the remaining [^{18}F]**7**, [^{18}F]**8** and [^{18}F]**9** degraded faster *in vivo*. Evidently, a longer circulating half-life can lead to better tumor image quality.

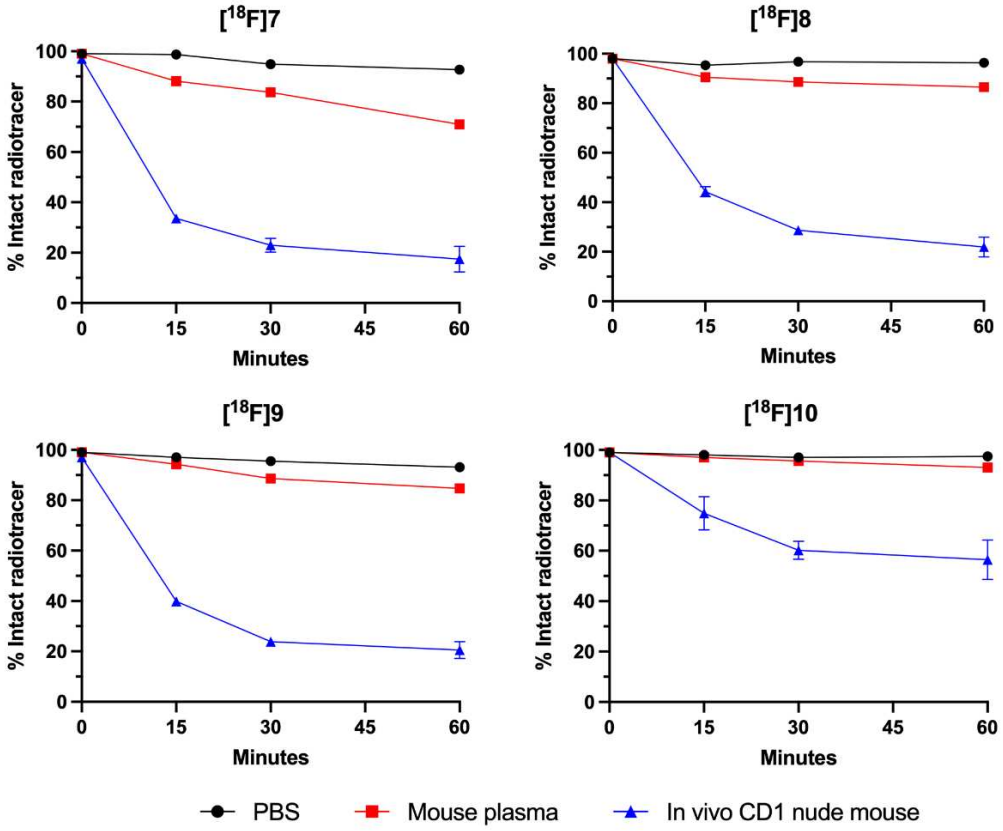

Figure 4. Radiotracer stability of [^{18}F]**7,** [^{18}F]**8,** [^{18}F]**9** and [^{18}F]**10** in PBS, mouse plasma and CD1 nude mice(n = 3 per timepoint).

IN VIVO BIODISTRIBUTION

The biodistribution profile of [^{18}F]**7**, [^{18}F]**8**, [^{18}F]**9** and [^{18}F]**10** was subsequently evaluated in healthy control mice (**Figure 5**). All radiotracers showed fast blood clearance with almost complete elimination from the blood pool at 60 min p.i., with [^{18}F]**9** and [^{18}F]**10** showing the lowest blood pool activity (0.13 ± 0.06%ID/g and 0.24 ± 0.03%ID/g, respectively). Significant uptake in the liver and intestine were also found for all the ligands, suggesting at least partial excretion via the hepatobiliary pathway. This would be comparable to the reported

biodistribution of ^{18}F-labeled FAPI radiotracers with somewhat lower hydrophilicity like the reported tracer **6**. As opposed to the latter, however, increased renal elimination was also observed for all tracers reported here, as demonstrated by the enhanced kidney and bladder uptake. Finally, the quaternary ammonium-containing ligand [^{18}F]**10** showed an almost neglectable uptake in the large intestine (0.38 ± 0.15%ID/g at 60 min p.i.), when compared with the other three ^{18}F-FAPI radioligands, confirming the hypothesis that linker polarity can be a relevant variable for FAPIs to improve biopharmaceutical properties. Clearly, the presence of increased abdominal radioligand uptake can cause a strong background signal and may limit the diagnostic imaging applications for tumors of the upper thoracic region in patients. While [^{18}F]**10** does not have the almost exclusive urinary clearance profile of the reported chelator-based [^{18}F]-labeled **3b**, it deserves mentioning that preclinical biodistribution studies have been reported to underestimate the urinary excretion of FAPIs in humans: this has for example also been the case for reference [^{68}Ga]**36**.[27]

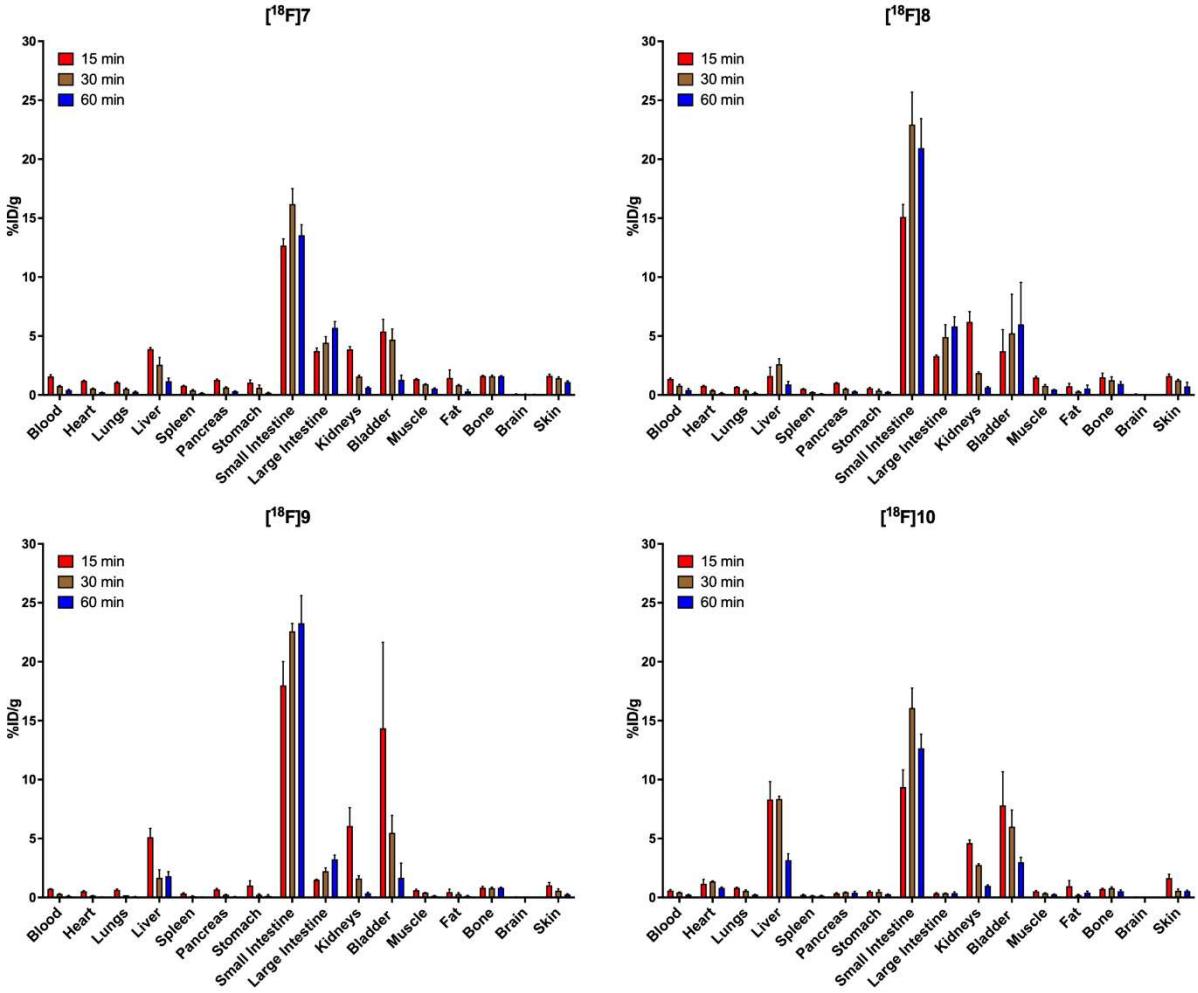

Figure 5. Tissue biodistribution of [^{18}F]**7,** [^{18}F]**8,** [^{18}F]**9** and [^{18}F]**10** in healthy CD1 nude mice. (n = 3 per timepoint)

IN VIVO PET/CT IMAGING AND BIODISTRIBUTION IN TUMOR-BEARING MICE

After evaluation of the pharmacokinetic properties and metabolic stability of the [^{18}F]-labeled radioligands, their potential for *in vivo* PET imaging in tumor-bearing mice was evaluated. The ^{18}F-labeled FAPI radioligands' performance vs. [^{68}Ga]Ga-DATA^{5m}.SA.FAPi and [^{68}Ga]Ga-DOTA-FAPI-04 was compared in U-87MG xenografts. U-87MG is a human glioblastoma-derived cell line that once inoculated *in vivo*, is known to express FAP within tumor xenografts, both on the cancer cells and in the stroma.[28] Tumor uptake for all radioligands, represented as TACs, is shown in **Figure 6**. Dynamic imaging over the course of 60 min p.i. for all four

radiofluorinated FAP ligands demonstrated an early peak uptake in the tumor followed by retention or slight decrease in the tumor over the duration of the PET scan. While [^{18}F]**7**, [^{18}F]**8** and [^{18}F]**9** showed relatively modest tumor uptake (< 3% ID/mL), [^{18}F]**10** had a remarkable and significantly higher tumor uptake compared to all the other ligands (10.16 ± 2.22% ID/mL at 60 min p.i.). In addition, uptake of [^{18}F]**10** in the tumor increased throughout the entire duration of the scan after an initial rapid uptake phase in the first minutes. In the same experiments, reference [^{68}Ga]**37** showed a later peak tumor uptake, reaching a maximum uptake at 8.8 min p.i. (5.46 ± 0.83%ID/mL), followed by a fast clearance from the tumor. In case of [^{68}Ga]**36**, sustained retention in the tumor was detected over the time period of the PET scan after a slow initial uptake in the tumor. Overall, these dynamically obtained tumor uptake values, correspond well with the *ex vivo* values, determined 60 min p.i. (**Figure 7**). Only for [^{68}Ga]**36**, a significantly higher tumor uptake is visible in the *ex vivo* measurement. This is at least in part explained by the presence of an outlier that had almost double tumor uptake compared to the other 3 isolated tumors of animals treated with [^{68}Ga]**36**. The latter is also reflected by the higher standard deviation for the corresponding mean tumor uptake value shown in **Figure 7**. In addition, all tracers displayed comparable organ biodistribution in the U87MG xenograft-bearing mice and in the healthy mice that were used in the pharmacokinetics study. The latter results were shown in **Figure 5**, while organ biodistribution data in xenograft-bearing mice are provided as Supporting Information (**Figure S1**).

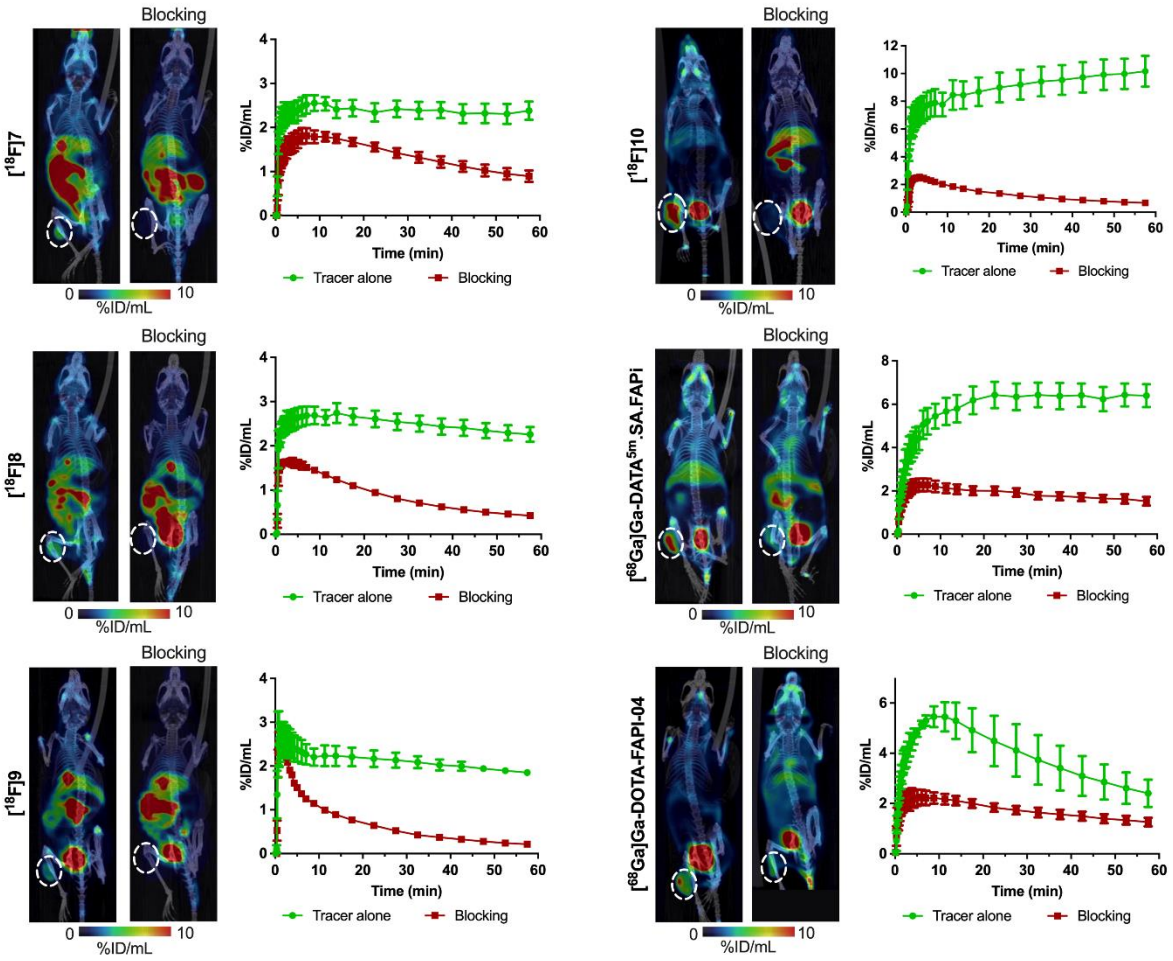

Figure 6. Representative coronal small-animal PET/CT images (0-60 min summed activity) and time-activity curves of U-87MG tumor–bearing animals, treated with a FAPI radioligand alone or pretreated with competitor **1** (5mg/kg), followed by injection with a FAPI radioligand. Time-activity curves are presented as mean ± SD.

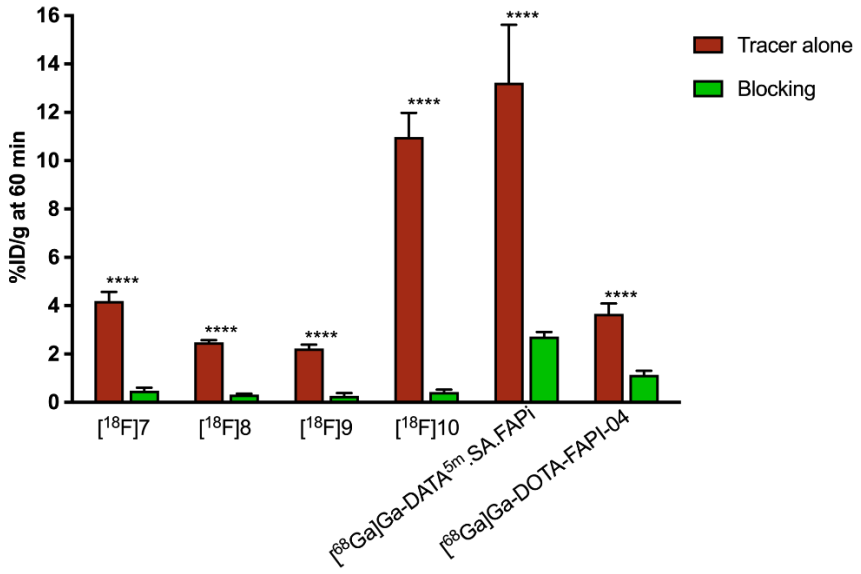

Figure 7. *Ex vivo* analysis of tumor uptake in U-89MG xenografts at 60 min p.i. Data are presented as mean ± SD. $p<0.0001$, significantly different from blocking.

Importantly, the specificity of [^{18}F]**7,** [^{18}F]**8,** [^{18}F]**9** and [^{18}F]**10** for FAP was confirmed with blocking experiments. Pre-injection of the specific FAP inhibitor **1** in mice bearing U-87MG tumors, led to a marked decrease in tumor uptake, demonstrating the specificity of all the tested radioligands for FAP (**Figures 6 and 7**). Of note, different background signals were present in the non-blocked and blocked animals treated with [^{18}F]10. We tentatively assign this observation to the fact that the tracer in the blocked animals is no longer retained in FAP^{+}-tissue. As a result, a larger fraction of the tracer stays in circulation, which leads to faster excretion. Because this excretion is partially urinary and partially hepatobiliary, an increased ^{18}F-signal in the gut is observed. A similar trend is present when looking at the liver and intestinal ^{18}F-signals in the biodistribution study in healthy mice (**Figure 5**). These animals also lack FAP^{+}-tumor tissue, which leads to decreased tissue retention of the tracer and, hence, faster clearance through the liver and the gut. This could explain the relatively high liver and intestinal signals. Interestingly, all four radiofluorinated ligands showed lower nonspecific

tumor uptake when compared to the ^{68}Ga-labeled FAPI ligands, which could be an advantage when imaging sites with lower FAP expression. In accordance with previous reports, high uptake of FAPI radioligands was also detected in bone structures, for example in the skull and bone joints, as demonstrated by the uptake in the mouse tibia of 4.33 ± 1.29%ID/g for **10** and 5.78 ± 1.77%ID/g for [^{68}Ga]**37** (detailed data provided in Supporting Information, **Figure S-1**) The other radiofluorinated FAPI ligands [^{18}F]**7**, [^{18}F]**8** and [^{18}F]**9** accumulated in bone structures to a much lower extent, and [^{68}Ga]**37** did not show increased accumulation in bone, potentially due to its fast clearance properties. Blocking experiments revealed that radioligand uptake in the bone was specific, as it was significantly decreased in the blocking experiment. This phenomenon has been attributed earlier to binding to FAP-expressing bone marrow stem cells (BMSC), which may serve as precursor cells of tumor stromal fibroblasts.[28] It has been shown that these mouse BMSCs have the ability to leave the bone marrow, circulate in the blood and home in on various tumor types and tissues undergoing remodeling. In U-87MG xenografts, the BMSCs can be recruited and become part of the tumor microenvironment.[29-32]

Overall, these data already indicate that [^{18}F]**10** has a very promising *in vivo* profile. Its high and persistent tumor uptake until at least 60 min. p.i. is a feature that is not present with [^{18}F]**7-9** or with FAPI-04 and other reported chelator-based FAPIs. It can tentatively be explained through 1) the somewhat higher plasma stability of [^{18}F]**10** compared with **7-9**, combined with 2) a higher lipophilicity and thus higher plasma protein binding compared to the chelator-based references. This could result in a prolonged circulation time, leading to continuous increase of [^{18}F]**10** in the tumor. Similar observations have been made for FAPIs equipped with an albumin-binding moiety.[33] To the best of our knowledge, results reported for non-chelator-based ^{18}F-labeled FAPI ligands have generally resulted in compounds with

suboptimal tumor uptake.[10] In addition, promising tumor-to-background ratios are achieved with [^{18}F]**10** (summarized in **Table 3**). These can also be attributed to aspects of its pharmacokinetic profile: less liver and intestinal uptake, and improved renal urinary excretion, when compared with [^{18}F]**7**, [^{18}F]**8** and [^{18}F]**9** (Shown in Supporting Information). Chelator-based compounds, nonetheless, are almost exclusively excreted through the kidneys and bladder in rodents. This is also confirmed in these experiments. However, some unexpected unspecific uptake of [^{68}Ga]**37** was also detected in the liver at the same extent as for [^{68}Ga]-**36** and [^{18}F]**10** (Shown in Supporting Information).

Table 3. Tumor-to-background ratios of FAPI radioligands in U-87MG xenografts at 60 min p.i.[(a),(b)]

Radiotracer	Tumor	Tumor-to-muscle	Tumor-to-blood	Tumor-to-small intestine	Tumor-to-liver
[^{18}F]**7**	4.17 ± 0.66	6.48 ± 2.35	5.01 ± 1.77	0.22 ± 0.06	1.64 ± 0.46
[^{18}F]**8**	2.49 ± 0.14	3.60 ± 1.37	6.58 ± 2.00	0.16 ± 0.03	2.37 ± 0.95
[^{18}F]**9**	2.23 ± 0.29	5.26 ± 0.82	6.56 ± 0.82	0.12 ± 0.02	1.67 ± 0.92
[^{18}F]**10**	10.98 ± 1.73	6.54 ± 1.36	6.35 ± 1.08	2.43 ± 0.12	4.77 ± 0.58
[^{68}Ga]Ga-DATA^{5m}.SA.FAPi ([^{68}Ga]**36**)	13.23 ± 4.14	6.46 ± 1.14	5.50 ± 1.90	3.91 ± 0.81	4.51 ± 0.93
[^{68}Ga]Ga-DOTA-FAPI-04 ([^{68}Ga]**37**)	3.67 ± 0.73	11.49 ± 3.81	5.06 ± 1.06	8.22 ± 1.94	1.87 ± 0.49

[(a)] Obtained from *ex vivo* quantitative biodistribution data of all mice used in the study (n=4/tracer).
[(b)] Values shown are means ± standard deviations of individual tumor-to-tissue ratios (n=4/tracer/tissue type).

As an alternative model for the U-87MG xenografts, we also generated human colon cancer HT29 xenografts for PET imaging studies using [^{18}F]**7**. Our team has used this model before, among others for the study of [^{68}Ga]**36**.[17] While HT29-cells are known to be FAP-negative, the

model shows strong infiltration of FAP-positive mouse CAFs.[34] In this tumor model, a similar tumor uptake was observed (1.86 ± 0.26%ID/mL at 60 min p.i., **Figure 8**).

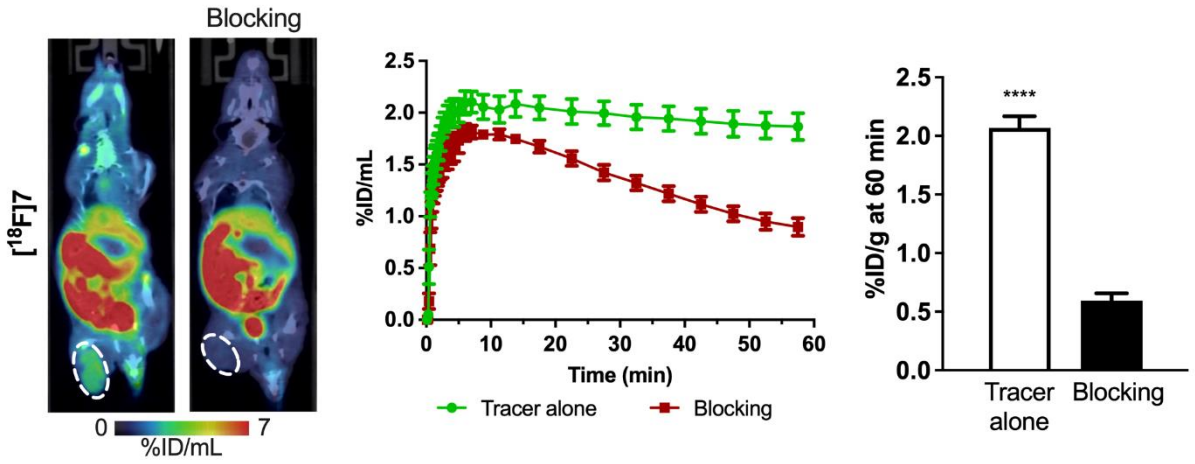

Figure 8. Representative coronal small-animal PET/CT images (0-60 min summed activity) and time-activity curves of HT29 tumor–bearing animals using [^{18}F]**7** and respective blocking experiments with competitor **1** (5mg/kg). Data presented as mean ± SD. $p<0.0001$, significantly different from blocking.

EX VIVO VALIDATION OF FAP EXPRESSION IN TUMORS

The regional distribution of FAP radioligands in the tumors was assessed by autoradiography of tumor slices, immediately after imaging. Autoradiographs showed a higher accumulation of [^{18}F]**7**, [^{18}F]**10** and [^{68}Ga]**37** in non-blocked tumors, when compared with tumors of mice pre-injected with **1**. Remarkably, the druglike [^{18}F]**7** and [^{18}F]**10** display a homogenous tumor uptake, while the chelator-based [^{68}Ga]**37** does not. The latter also shows highest uptake in the rim of the tumor, and relatively less core uptake. This behavior could point in the direction of a lower tissue permeability of chelator-based molecules. In overall agreement with radioligand uptake, FAP immunoreactivity was increased in both HT29 and U-87MG xenografts (**Figure 9**). To compare the expression profile of FAP in both the HT29 and the U-

87MG xenografts, cryosections of both tumors were also stained for alpha-smooth muscle actin (α-SMA). As both FAP and α-SMA are the most specific markers for cancer-associated fibroblasts (CAFs), they can be used to distinguish FAP expression in the tumor stroma versus in the cancer cells themselves. As expected, (*vide supra*), a different FAP expression pattern between both the HT29 and U-87MG xenograft model is present. (**Figure 10, Entry B**) In the HT29 model, FAP expression is restricted to the tumor stroma and hence a clear co-localization between FAP and α-SMA expression is visible (yellow overlay). No FAP staining is visible on the HT29 colorectal adenocarcinoma cancer cells. On the other hand, in the U-87MG model FAP is expressed both in the tumor stroma (and co-localizing with α-SMA), but also on the glioblastoma cancer cells.

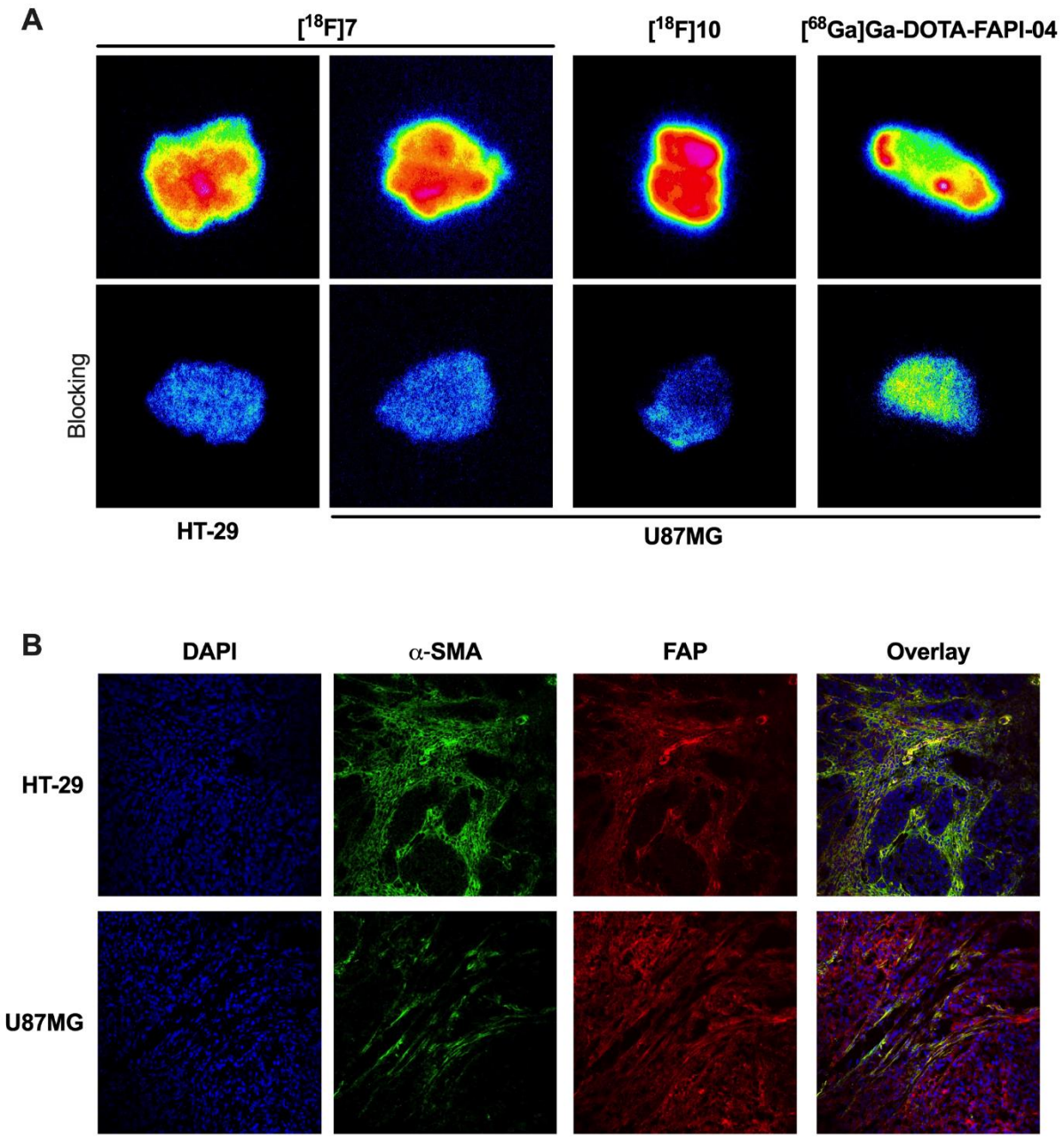

Figure 9. *Ex vivo* evaluation of radiotracer uptake and FAP expression in whole-tumor sections. Representative pseudo color autoradiography (A) and confocal microscopy images (B) of adjacent HT29 and U-87MG whole-tumor slices stained for FAP and α-SMA (20x magnification).

Finally, we also performed *ex vivo* FAP quantification on the tumors of animals treated with the individual tracers. Noteworthy, for [^{18}F]**7**, both the tumors obtained from the U-87MG (n=4) and HT29 (n=4) mice were used. In the tumors of animals treated with [^{18}F]**7**, [^{18}F]**10** and [^{68}Ga]**37**, FAP was quantified by means of immunohistochemistry (IHC), using % FAP positive

tumor area ('FAP positivity') as a read-out. As expected, U-87MG tumors showed an increased FAP positive tumor area (75.9 ± 11.6%) when compared to HT29 tumors (32.1 ± 12.6%, $p<0.0001$). This is illustrated in **Figure 10, Entry A**: in the graph for [^{18}F]**7**, the 4 data points with the lowest FAP positivity correspond to the HT29 tumors, while the 4 data points with highest FAP positivity correspond to the U-87MG tumors The graph also shows a satisfactory correlation between FAP and [^{18}F]**7** tumor uptake, both for HT29 and U-87MG tumors ($r=0.949$, $p=0.0003$). Comparably, also the uptake of [^{18}F]**10** ($r=0.967$, $p=0.032$) was highly correlated to FAP expression. In contrast, animals injected with [^{68}Ga]**37** showed a poorer correlation between mean tumor radioactivity and FAP expression.

For the quantification of FAP in tumors from animals treated with [^{18}F]**8**, [^{18}F]**9** and [^{68}Ga]**36**, FAP was quantified based on FAP-activity in tumor lysates. This alternative technique, which we have used earlier for *ex vivo* quantification of FAP, was chosen because of technical problems with obtaining suitable cryosections for IHC quantification.[7] Gratifyingly, however, animals injected with [^{18}F]**9** ($r=0.919$, $p=0.001$), [^{18}F]**8** ($r=0.814$, $p=0.014$) and [^{68}Ga]**36** ($r=0.891$, $p=0.0071$) also showed a good correlation between tumor uptake and FAP activity in the tumors (**Figure 10, Entry B**).

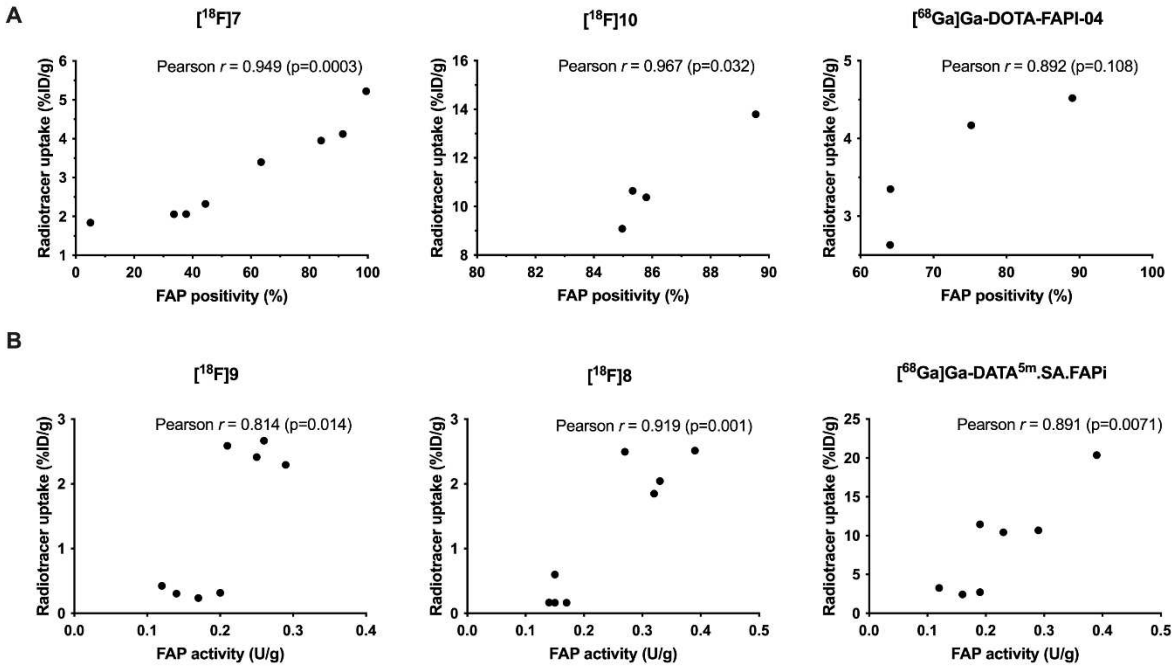

Figure 10. Correlation analysis of radiotracer uptake with histological measure of FAP expression (A) and with FAP activity in whole tumor sections (B). FAP expression (A) and activity (B) were compared with tumor-associated radioactivity measured *ex vivo* (n = 4 - 8 tumors per group). Pearson correlation values (r) and two-tailed *p* values are shown in the top right corner of charts.

CONCLUSION

Four novel fluorinated radioligands targeting the fibroblast activation protein (FAP) were synthesized and analyzed. These radioligands were developed using our very potent and specific FAP inhibitor, UAMC1110. The ^{18}F-labeled FAPIs in question were equipped with short polar linkers that were covalently bonded to the ^{18}F-label. This modification resulted in an enhancement of their druglike characteristics. In this particular series, [^{18}F]10 exhibited notable hydrophilicity, excellent metabolic stability, and a favorable pharmacokinetic profile *in vivo*. This is attributed to the presence of a quaternary ammonium linker in the compound's structure. The new ligand exhibited both selective and prolonged tumor uptake. Due to its rapid clearance and minimal buildup in non-target tissue, positron emission tomography (PET)

imaging using [^{18}F]**10** yielded images characterized by elevated ratios between target and non-target regions and was superior to all other ligands investigated in this study.

In summary, the preclinical data presented in this study, positions [^{18}F]10 as an excellent and promising alternative to the well-known chelator-based FAPIs, such as [^{68}Ga]Ga-DATA^{5m}-SA.FAPI and in particular [^{68}Ga]Ga-FAPI-04. Advantages of [^{18}F]**10** include the preparation using an automated radiolabeling procedure, which enables a GMP compliant synthesis, and the potential for upscaling of the production and distribution to smaller nuclear medicine centers. Taken together, these data support the pursuit of [^{18}F]**10** and analogues for clinical development.

EXPERIMENTAL SECTION

Chemistry. Reagents were obtained from commercial sources and were used without further purification. Characterization of all compounds was done with ^{1}H and ^{13}C NMR and mass spectrometry. ^{1}H and ^{13}C NMR spectra were recorded on a 400 MHz Bruker Avance III Nanobay spectrometer with Ultrashield working at 400 and 100 MHz, respectively, and analyzed by use of MestReNova analytical chemistry software. Chemical shifts are in ppm, and coupling constants are in hertz (Hz). The UPLC (ultraperformance liquid chromatography), used to quantify the purity of the products was an ACQUITY UPLC H-Class system with a TUV detector Waters coupled to an MS detector Waters QDa. An Acquity UPLC BEH C18 1.7 µm (2.1 mm × 50 mm) column was used and as eluent a mixture of 0.1% FA in H_2O, 0.1% FA in ACN, H_2O, and ACN. The wavelengths for UV detection were 254 and 214 nm. Key target compounds for the activity were analyzed by high resolution mass spectrometry: 10 µL of each sample (concentration = 10−5 M) was injected using the CapLC system (Waters, Manchester, UK) and

electrosprayed using a standard electrospray source. Samples were injected with an interval of 5 min. Positive ion mode accurate mass spectra were acquired using a Q-TOF II instrument (Waters, Manchester, UK). The MS was calibrated prior to use with a 0.2% H_3PO_4 solution. The spectra were lock mass corrected using the known mass of the nearest H_3PO_4 cluster. When necessary, flash column chromatography was performed on a Biotage ISOLERA One flash system equipped with an internal variable dual-wavelength diode array detector (200−400 nm). For normal phase purifications, Biotage Sfär cartridges (5−100 g, flow rate of 10−100 mL/min) were used, and reverse phase purifications were done making use of Büchi C18 cartridges (4−30 g, flow rate of 10−50 mL/min). Dry sample loading was done by self-packing sample cartridges using Celite 545. Gradients used varied for each purification.

The following sections comprise the synthetic procedures and analytical data for all compounds reported in this manuscript. Every reaction was performed under N_2 atmosphere if not stated otherwise. A synthetic procedure that was used in the preparation of several intermediates and final products is summarized here as “General Procedure”. Target compounds were obtained with a purity > 95% and as amorphous solids unless stated otherwise.

(((2-Methoxypropane-1,3-diyl)bis(oxy))bis(methylene))dibenzene (12)

A 100 mL round bottom flask was charged with 1,3-dibenzyloxy-2-propanol (5 g, 18.36 mmol) and 50 mL DMF. Then, NaH (0.485 g, 1.1 eq) and iodomethane (1.2 eq) was added at 0°C and the reaction mixture was stirred at room temperature for 2 h. After consumption of starting material (UPLC monitoring) the reaction was quenched with slush and 1 M HCl (3 x 20 mL) following extracted with EtOAc (3 x 20 mL). The combined organic layers were washed with brine (3 x 20 ml), dried over Na_2SO_4, filtered and the solvent was evaporated under reduced pressure. The residue was purified by silica gel column chromatography eluting with 20 %

EtOAc / *n*-heptane and the title compound was obtained as a colourless oil (yield: 72 %). **^{1}H NMR** (400 MHz, DMSO-d_6, δ): 3.33 (s, 3H), 3.50 (m, 5H), 4.48 (s, 4H), 7.30 (m, 10H). **^{13}C NMR** (100 MHz, DMSO-d_6, δ), 57.2, 69.4, 72.3, 78.7, 127.4, 127.5, 128.3, 138.4. **MS** t_R 2.02 min, UPLC MS (ESI) m/z 309.1 $[M+Na]^+$

2-Methoxypropane-1,3-diol (13)

A 100 mL round bottom flask was charged with (((2-methoxypropane-1,3-diyl)bis(oxy))bis(methylene))dibenzene (7.1 g, 24.79 mmol) and 50 mL MeOH . Afterwards, a catalytic amount of $Pd(OH)_2$ was added and the reaction mixture was stirred under H_2 atmosphere until the starting compound was consumed (TLC monitoring). The H_2 atmosphere was then replaced by N_2, the reaction mixture filtered over celite and all volatiles were removed under vacuo. The title compound was obtained as a colourless oil (quantitative yield). **^{1}H NMR** (400 MHz, DMSO-d_6, δ): 3.11 (p, *J* = 5.2 Hz, 1H), 3.30 (s, 3H), 3.39 (m, 4H), 4.51 (t, *J* = 5.7 Hz 2H). **^{13}C NMR** (100 MHz, DMSO-d_6, δ), 56.9, 60.4, 82.9.

2-Methoxypropane-1,3-diyl bis(4-methylbenzenesulfonate) (14)

A 100 mL round bottom flask was charged with 2-methoxypropane-1,3-diol (2.65 g, 24.97 mmol), pyridine (4 eq) and dichloromethane (40 ml). Following, *p*-tosyl chloride (2.1 eq) was added in one portion at 0 °C and the reaction mixture was stirred at room temperature. After consumption of starting materials (UPLC monitoring), the reaction was quenched with slush and 1 M HCl (3 x 10 mL). It was then extracted with dichloromethane (3 x 20 mL). The combined organic layers were washed with brine (3 x 10 ml), dried over Na_2SO_4, filtered and

the solvent was eliminated under reduced pressure. The residue was purified by silica gel column chromatography eluting with 20-40 % EtOAc / *n*-heptane and the title compound was obtained as a white solid (59 % yield). **^{1}H NMR** (400 MHz, DMSO-d_6, δ): 2.42 (s, 6H), 3.13 (s, 3H), 3.60 (m, 1H), 3.94 (dd, *J* = 5.6, 10.9 Hz, 2H), 4.07 (dd, *J* = 3.7, 10.9 Hz, 2H), 7.47 (d, *J* = 8.0 Hz, 4H), 7.74 (d, *J* = 8.0 Hz, 4H). **^{13}C NMR** (100 MHz, DMSO-d_6, δ), 21.1, 57.1, 68.2, 75.5, 127.7, 130.2, 131.9, 145.2. **MS** t_R 1.96 min, UPLC MS (ESI) m/z 432.1 $[M+NH_4]^+$

2-Hydroxypropane-1,3-diyl bis(4-methylbenzenesulfonate) (15)

A 50 mL round bottom flask was charged with glycerin (1 g, 10.86 mmol), 4-dimethylaminopyridine (0.25 eq) and 10 mL of dry pyridine. Afterwards, at -20 ℃, *p*-tosyl chloride (2.2 eq) in 10 mL of dry pyridine was added dropwise. The reaction was kept under -20 ℃ for 36 hours. The formed precipitate was filtered and the filtrate washed with 5 mL cold pyridine. Following filtration, the mixture was quenched with slush and diluted with 40 mL of dichloromethane. The diluted mixture was washed with 1 M HCl (5 x 20 mL). The organic phase was dried over Na_2SO_4, filtered and the solvent was eliminated under reduced pressure to give a residue. This was purified by silica gel column chromatography, eluting with 40-60 % EtOAc / *n*-heptane and the title compound obtained as a colorless oil (69 % yield). **^{1}H NMR** (400 MHz, DMSO-d_6, δ): 2.42 (s, 6H), 3.87 (m, 4H), 4.07 (m, 1H), 5.65 (d, *J* = 4.5 Hz, 1H), 7.47 (d, *J* = 7.4 Hz, 4H), 7.74 (d, *J* = 8.4 Hz, 4H). **^{13}C NMR** (100 MHz, DMSO-d_6, δ), 55.8, 57.5, 59.9, 73.8, 104.6, 136.6, 152.8. **MS** t_R 1.44 min, UPLC MS (ESI) m/z 278.2 $[M+Na]^+$ (81%).

2-((Tetrahydro-2H-pyran-2-yl)oxy)propane-1,3-diyl bis(4-methylbenzenesulfonate) (16)

A 50 mL round bottom flask was charged with 2-hydroxypropane-1,3-diyl-bis(4-methylbenzenesulfonate) (1.3 g, 3.25 mmol), pyridinium *p*-toluenesulfonate (4 eq) and 40 mL of dry CH_2Cl_2. Afterwards, dihydropyran (4 eq) was added to the reaction mixture and stirred at 40 ℃ until the starting compound was consumed (UPLC monitoring). Next, all volatiles were evaporated and the mixture was diluted with 50 mL of EtOAc. The formed precipitate was removed and the filtrant was evaporated under reduced pressure to give a crude that that was purified by silica gel column chromatography. The elution was carried out with 20 % EtOAc / *n*-heptane and the title compound was obtained as a white solid (89 % yield). **^{1}H NMR** (400 MHz, DMSO-d_6, δ): 1.38, (m, 6H), 2.42 (s, 6H), 3.27 (m, 1H), 3.53 (m, 1H), 3.99 (m, 5H), 5.54 (d, *J* = 2.7 Hz, 1H), 7.48 (d, *J* = 8.1 Hz, 4H), 7.75 (d, *J* = 8.5 Hz, 4H). **^{13}C NMR** (100 MHz, DMSO-d_6, δ), 18.5, 21.1, 24.8, 29.8, 61.2, 68.4, 69.2, 70.8, 97.14, 127.7, 127.7, 130.2, 130.2, 131.8, 131.9, 145.2. **MS** t_R 1.44 min, UPLC MS (ESI) m/z 507.2 $[M+Na]^+$.

Methyl 6-hydroxyquinoline-4-carboxylate (17)

A 100 mL roundbottom flask was charged with 6-hydroxyquinoline-4-carboxylic acid (1.1 g, 5.81 mmol) and 23.5 mL of MeOH (100 eq). After the temperature of the mixture decreased to 0 ℃, thionyl chloride (10 eq) was added dropwise. Next, the reaction was refluxed until consumption of the starting compound (UPLC monitoring). After all volatiles were evaporated via rotavap, the crude was washed with cold acetone and dried under high *vacuo*. The title compound was obtained as dark red solid (80% yield). **^{1}H NMR** (400 MHz, DMSO-d_6, δ): 3.96 (s, 3H), 7.39 (dd, *J* = 2.6, 9.0 Hz, 1H), 7.86 (d, *J* = 3.4 *Hz*, 1H), 7.97 (m, 2H), 10.36 (s, 1H). **^{13}C**

NMR (100 MHz, DMSO-d_6, δ), 53.7, 107.18, 123.3, 125.8, 126.9, 127.5, 137.2, 138.5, 143.2, 159.2, 165.7.

Methyl 6-(2-methoxy-3-(tosyloxy)propoxy)quinoline-4-carboxylate (18a)

A 50 mL round bottom flask was charged with methyl 6-hydroxyquinoline-4-carboxylate (0.4 g, 1.969 mmol), cesium carbonate (5 eq) and 10 mL of dry DMF. After 15 min stirring at 40 ℃, 2-methoxypropane-1,3-diyl bis(4-methylbenzenesulfonate) (1.2 eq) was added to the mixture at room temperature and the reaction was heated up again to 40 ℃. After the starting materials were consumed (UPLC monitoring). the reaction was quenched with slush and 1 M HCl (10 mL). It was then extracted with EtOAc (3 x 10 mL). The combined organic layers were washed with brine (3 x 10 ml), dried over Na_2SO_4, filtered and the solvent was eliminated under reduced pressure. The residue was purified by silica gel column chromatography eluting with 10-60 % EtOAc / *n*-heptane and the title compound was obtained as a pale yellow solid (52 % yield). **^{1}H NMR** (400 MHz, DMSO-d_6, δ): 2.29 (s, 3H), 3.33 (s, 3H), 3.83 (p, *J*= 5.1 Hz, 1H), 3.99 (s, 3H), 4.11 (d, *J* = 5.1 Hz, 2H), 4.18 (dd, *J* = 3.5, 10.7 Hz, 1H), 4.32 (dd, *J* = 5.1, 10.7 Hz, 1H), 7.37 (d, *J* = 8.0 Hz, 2H), 7.41 (dd, *J* = 2.8, 9.2 Hz, 1H), 7.78 (d, *J* = 8.3 Hz, 2H), 7.94 (d, *J* = 4.4 Hz, 1H), 7.98 (d, *J* = 2.8 Hz, 1H), 8.04 (d, *J* = 9.2 Hz, 1H), 8.90 (d, *J* = 4.4 Hz, 1H). **^{13}C NMR** (100 MHz, DMSO-d_6, δ), 21.0, 52.8, 57.3, 65.8, 68.8, 76.1, 104.3, 122.2, 122.7, 125.5, 127.64, 130.12, 131.3, 132.0, 132.7, 144.8, 144.9, 147.7, 157.2, 166.3. **MS** t_R 1.88 min, UPLC MS (ESI) m/z 446.2 $[M+H]^+$.

Methyl 6-(2-((tetrahydro-2H-pyran-2-yl)oxy)-3-(tosyloxy)propoxy)quinoline-4-carboxylate (18b)

A 10 mL round bottom flask was charged with methyl 6-hydroxyquinoline-4-carboxylate (0.12 g, 0.591 mmol), cesium carbonate (5 eq) and 5 mL of dry DMF. After 15 min of stirring at 40

°C 2-((tetrahydro-2H-pyran-2-yl)oxy)propane-1,3-diyl bis(4-methylbenzenesulfonate) (0.315 g, 0,650 mmol) was added to the mixture at room temperature and reaction was heated up again to 40 °C. After the starting materials were consumed (UPLC monitoring), the reaction was quenched with slush and extracted with EtOAc (3 x 10 mL). The combined organic layers were washed with brine (3 x 5 ml), dried over Na_2SO_4, filtered and the solvent was eliminated under reduced pressure. This yielded a residue that was purified by silica gel column chromatography, eluting with 5-40 % EtOAc / *n*-heptane. The title compound was obtained as a pale yellow solid (49 % yield). **^{1}H NMR** (400 MHz, DMSO-d_6, δ): 1.42 (brs, 4H), 1.59 (brs, 2H), 2.29 (s, 3H), 3.39 (s, 3H), 4.21 (m, 5H), 7.37 (d, *J* = 8.0 Hz, 2H), 7.41 (dd, *J* = 2.7, 9.1 Hz, 1H), 7.78 (d, *J* = 8.3 Hz, 2H), 7.93 (d, *J* = 4.5 Hz, 1H), 7.99 (d, *J* = 2.7 Hz, 1H), 8.02 (d, *J* = 9.2 Hz, 1H), 8.90 (d, *J* = 4.5 Hz, 1H). **^{13}C NMR** (100 MHz, DMSO-d_6, δ), 18.7, 21.0, 24.9, 30.1, 52.8, 61.3, 64.9, 66.1, 69.3, 71.5, 97.3, 104.4, 122.3, 122.7, 125.5, 127.7, 130.1, 131.3, 131.9, 132.7, 144.9, 147.8, 157.3, 166.3. **MS** t_R 2.02 min, UPLC MS (ESI) m/z 516.2 $[M+H]^+$, m/z 538.1 $[M+Na]^+$.

6-(2-Methoxy-3-(tosyloxy)propoxy)quinoline-4-carboxylic acid (19a)

A 10 mL cylindrical flask was charged with methyl 6-(2-methoxy-3-(tosyloxy)propoxy)quinoline-4-carboxylate (0.48 g, 1.077 mmol) and 5 mL of MeOH. Afterwards, NaOH (5 eq) was added and the mixture stirred at 40 °C until the starting compound was consumed (UPLC monitoring). Subsequently, the pH of the reaction mixture was adjusted to 6 by adding the necessary amount of 1 M HCl at room temperature. The formed precipitate was collected by filtration through a glass filter and dried under high vacuum. The title compound was obtained as pale yellow solid (71 % yield). **^{1}H NMR** (400 MHz, DMSO-d_6, δ): 2.30 (s, 3H), 3.32 (s, 3H), 3.82 (p, *J*= 4.9 Hz, 1H), 4.08 (d, *J* = 5.4 Hz, 2H), 4.18 (dd, *J* = 5.3, 10.7 Hz, 1H), 4.32 (dd, *J* = 3.4, 10.7 Hz, 1H), 7.37 (m, 3H), 7.77 (d, *J* = 8.1 Hz, 2H), 7.89

(d, *J* = 4.1 Hz, 1H), 7.99 (d, *J* = 9.3 Hz, 1H), 8.10 (d, *J* = 2.9 Hz, 1H). **^{13}C NMR** (100 MHz, DMSO-*d*$_6$, δ), 21.5, 57.7, 66.2, 69.2, 76.5, 105.19, 122.43, 123.1, 126.4, 128.1, 130.6, 131.6. 132.5, 145.3, 145.5, 148.25, 157.4, 168.1. **MS** t_R 1.44 min, UPLC MS (ESI) m/z 430.2 $[M-H]^-$ (82%).

6-(2-((Tetrahydro-2*H*-pyran-2-yl)oxy)-3-(tosyloxy)propoxy)quinoline-4-carboxylic acid (19b)

A 10 mL cylindrical flask was charged with methyl 6-(2-((tetrahydro-2H-pyran-2-yl)oxy)-3-(tosyloxy)propoxy)quinoline-4-carboxylate (0.12 g, 0.233 mmol) and 5 mL of dry MeOH. Afterwards NaOH (5 eq) was added and the mixture was stirred at 40 °C until the starting compound was consumed (UPLC monitoring). Following, 0.5 mL of EtOAc was added and the pH of the reaction mixture was adjusted to 6 by adding the necessary amount of 1 M HCl at room temperature. The formed precipitate was collected by filtration through a glass filter and dried under high vacuum. The title compound was obtained as a white solid (86 % yield). **^{1}H NMR** (400 MHz, DMSO-*d*$_6$, δ): 1.41 (brs, 4H), 1.58 (brs, 2H), 2.30 (s, 3H), 4.19 (m, 5H), 7.37 (d, *J* = 7.5 Hz, 3H), 7.77 (d, *J* = 8.1 Hz, 2H), 7.92 (d, *J* = 4.3 Hz, 1H), 8.01 (d, *J* = 9.3 Hz, 1H), 8.09 (d, *J* = 1.9 Hz, 1H), 8.87 (d, *J* = 4.4 Hz, 1H), 13.79 (brs, 1H). **^{13}C NMR** (100 MHz, DMSO-*d*$_6$, δ), 19.1, 21.5, 25.3, 30.5, 62.0, 66.6, 70.4, 71.9, 72.3, 97.8, 105.4, 122.4, 123.4, 126.5, 128.2, 130.6, 131.6, 132.4, 145.4, 145.5, 148.5, 157.5, 168.4. **MS** t_R 1.68 min, UPLC MS (ESI) m/z 502.2 $[M+H]^+$, m/z 546.1 $[M+2Na-H\ ]^+$ (94%).

3-((4-((2-((*S*)-2-Cyano-4,4-difluoropyrrolidin-1-yl)-2-oxoethyl)carbamoyl)quinolin-6-yl)oxy)-2-methoxypropyl 4-methylbenzenesulfonate (20)

The compound was prepared according to **General procedure A** using 6-(2-methoxy-3-(tosyloxy)propoxy)quinoline-4-carboxylic acid (0,33 g, 0.765 mmol) and (*S*)-2-(2-cyano-4,4-

difluoropyrrolidin-1-yl)-2-oxoethan-1-aminium 4-methylbenzenesulfonate (1.1 eq) as reactants. After purification of the residue by silica gel column chromatography, eluting with 0-6 % MeOH / CH_2Cl_2, the title compound was obtained as a white solid (33 % yield). **^{1}H NMR** (400 MHz, DMSO-*d_6*, δ): 2.31 (s, 3H), 2.91 (m, 2H), 3.32 (s, 3H), 3.82 (brs, 1H), 4.18 (m, 8H), 5.13 (m, 1H), 7.34 (dd, *J* = 4.5, 9.4 Hz, 1H), 7.40 (d, , *J* = 8.0 Hz, 2H), 7.53 (d, *J* = 4.5 Hz, 1H), 7.79 (m, 3H), 7.97 (d, *J* = 9.2 Hz, 1H), 8.83 (d, *J* = 4.2 Hz, 1H), 9.11 (t, *J* = 5.5 Hz, 1H). **^{13}C NMR** (100 MHz, DMSO-*d_6*, δ), 21.9, 32.2, 37.4 (t, J_{C-T} 27), 42.3, 45.17 (d, J_{C-T} 7), 52.2 (t, J_{C-T} 31), 58.2 (d, J_{C-T} 5), 66.8 (d, J_{C-T} 7), 69.8, 77.0 (d, J_{C-T} 5), 105.6, 118.7, 120.2, 123.3, 126.3, 127.8 (t, J_{C-T} 245), 128.6, 131.0, 131.7, 132.9, 141.7, 145.2, 145.9, 148.6, 157.4 (d, J_{C-T} 4), 168.4, 169.0.

3-((4-((2-((S)-2-Cyano-4,4-difluoropyrrolidin-1-yl)-2-oxoethyl)carbamoyl)quinolin-6-yl)oxy)-2-((tetrahydro-2H-pyran-2-yl)oxy)propyl 4-methylbenzenesulfonate (21)

Compound was prepared according to **General procedure A** using 6-(2-((tetrahydro-2H-pyran-2-yl)oxy)-3-(tosyloxy)propoxy)quinoline-4-carboxylic acid (0.045 g, 0.090 mmol) and (*S*)-2-(2-cyano-4,4-difluoropyrrolidin-1-yl)-2-oxoethan-1-aminium 4-methylbenzenesulfonate (1.1 eq) as reactants. After purification of the residue by silica gel column chromatography eluting with 0-6 % MeOH / CH_2Cl_2, the title compound was obtained as a white solid (49 % yield). **^{1}H NMR** (400 MHz, DMSO-*d_6*, δ): 1.41 (brs, 4H), 1.58 (brs, 2H), 2.90 (m, 2H), 3.37 (s, 3H), 3.43 (m, 1H), 3.37 (m, 1H), 4.20 (m, 9H), 4.83 (m, 1H), 5.15 (m, 1H), 7.35 (dd, *J* = 2.6, 9.2 Hz, 1H), 7.39 (d, *J* = 8.1 Hz, 2H), 7.53 (d, *J* = 4.3 Hz, 1H), 7.78 (m, 3H), 7.98 (d, *J* = 9.3 Hz, 1H), 8.83 (d, *J* = 4.3 Hz, 1H), 9.10 (t, *J* = 5.8 Hz, 1H). **^{13}C NMR** (100 MHz, DMSO-*d_6*, δ), 19.1, 21.4, 25.3, 30.5, 31.7, 36.5, 36.8, 37.0, 41.8, 51.3, 51.6, 51.9, 61.7, 61.9, 66.6, 66.7, 71.9, 97.8, 97.9, 105.2, 118.1, 119.7, 122.7, 125.7, 128.1, 131.2, 132.3, 141.1, 144.6, 145.45, 148.1, 156.9, 167.8, 168.5.

6-(3-Fluoro-2-methoxypropoxy)quinoline-4-carboxylic acid (22a)

A 10 mL cylindrical flask was charged with methyl 6-(2-methoxy-3-(tosyloxy)propoxy)quinoline-4-carboxylate (0.1 g, 0.224 mmol), 2 mL of acetonitrile and tetrabutylammonium fluoride (5 eq). The reaction was stirred at 80 °C until consumption of the starting compound (UPLC monitoring). Afterwards, all volatiles were evaporated and crude was diluted with 5 mL of dichloromethane, washed with 1 M HCl (5 x 2mL) and dried over Na_2SO_4. The latter was filtered off and the solvent was eliminated under reduced pressure. The obtained residue was purified by silica gel column chromatography eluting with 0-6 % MeOH / CH_2Cl_2 and the title compound was obtained as a yellow solid (16 % yield). **MS** t_R 0.91 min, UPLC MS (ESI) m/z 278.2 $[M-H]^-$.

6-(3-Fluoro-2-((tetrahydro-2H-pyran-2-yl)oxy)propoxy)quinoline-4-carboxylic acid (22b)

A 10 mL cylindrical flask was charged with methyl 6-(2-((tetrahydro-2H-pyran-2-yl)oxy)-3-(tosyloxy)propoxy)quinoline-4-carboxylate (0.15 g, 0.291 mmol), 3 mL of acetonitrile and tetrabutylammonium fluoride (5 eq). The reaction was stirred at 80 °C until consumption of the starting compound (UPLC monitoring). Afterwards, all volatiles were evaporated and the crude was diluted with 5 mL of dichloromethane washed with H_2O (5 x 2mL), dried over Na_2SO_4, filtered and the solvent was eliminated under reduced pressure. The obtained residue was purified by silica gel column chromatography. The title compound was eluted with 0-6 % MeOH / dichloromethane and the title compound was obtained as a yellow solid (9 % yield). **^{1}H NMR** (400 MHz, DMSO-d_6, δ): 1.62 (m, 6H), 3.47 (m, 1H), 3.81 (m, 1H), 4.22 (m, 3H), 4.62 (d, *J* = 3.5 Hz, 1H), 4.74 (d, *J* = 3.8 Hz, 1H), 4.93 (s, 1H), 7.51 (dd, *J* = 2.9, 9.4 Hz, 1H), 7.89 (d, *J* = 4.5 Hz, 1H), 8.02 (d, *J* = 9.5 Hz, 1H), 8.21 (d, *J* = 2.7 Hz, 1H), 8.86 (d, *J* = 4.5 Hz, 1H), 13.77 (brs,

1H). **^{13}C NMR** (100 MHz, DMSO-d_6, δ), 19.4, 25.4, 30.7, 61.9, 66.8, 73.1 (d, J_{C-T} 19), 82.8, 84.5, 97.9, 105.3, 122.6, 123.2, 126.2, 131.8, 134.5, 145.4, 148.3, 157.8, 168.0. **MS** t_R 1.25 min, UPLC MS (ESI) m/z 350.2 $[M+H]^+$.

***N*-(2-((S)-2-Cyano-4,4-difluoropyrrolidin-1-yl)-2-oxoethyl)-6-(3-fluoro-2-methoxypropoxy) quinoline-4-carboxamide (23)**

The compound was prepared according to **General procedure A** using 6-(3-fluoro-2-methoxypropoxy)quinoline-4-carboxylic acid (0.025 g, 0.090 mmol) and (*S*)-2-(2-cyano-4,4-difluoropyrrolidin-1-yl)-2-oxoethan-1-aminium 4-methylbenzenesulfonate (1.1 eq) as reactants. After purification of the residue by silica gel column chromatography eluting with 0-6 % MeOH / CH_2Cl_2, the title compound was obtained as a white solid (24 % yield). ^{1}H NMR (400 MHz, $CDCl_3$-d_1, δ): 2.74 (p, *J* = 8.5 Hz, 2H), 3.53 (s, 3H), 4.01 (m, 6H), 4.33 (dt, *J* = 5.2 17.3 Hz, 1H), 4.57 (m, 1H), 4.70 (m, 1H), 4.97 (t, *J* = 6.7 Hz, 1H), 7.33 (m, 2H), 7.43 (brs, 1H), 7.57 (s, 1H), 7.90 (d, *J* = 9.6 Hz, 1H), 8.62 (d, *J* = 4.1 Hz, 1H). ^{13}C NMR (100 MHz, $CDCl_3$-d_1, δ), 36.9 (t, J_{C-T} 25), 42.0, 44.3, 51.9 (t, J_{C-T} 29), 58.4, 66.4 (dd, J_{C-T} 7, 28), 77.8 (dd, J_{C-T} 7, 19), 81.4 (d, J_{C-T} 5), 83.1 (d, J_{C-T} 5), 10.35, 116.2, 119.1, 123.12, 125.30, 131.18, 139.1, 144.8, 147.2, 157.4, 167.6, 167.9. MS t_R 1.56 min. UPLC MS (ESI) m/z 449.3 $[M-H]^-$, m/z 495.3 $[M+FA-H]^-$. HRMS(ESI) $C_{21}H_{20}F_3N_4O_4$ $[M-H]^-$, calcd 449.4108; found 449.4103

***N*-(2-((S)-2-Cyano-4,4-difluoropyrrolidin-1-yl)-2-oxoethyl)-6-(3-fluoro-2-hydroxypropoxy) quinoline-4-carboxamide (24)**

6-(((4S,5S)-2,2-Dimethyl-5-((tosyloxy)methyl)-1,3-dioxolan-4-yl)methoxy)quinoline-4-carboxylic acid (0.21 g, 0.431 mmol) and *O*-(7-azabenzotriazol-1-yl)-*N*,*N*,*N*',*N*'-

tetramethyluronium hexafluorophosphate (0.180 g, 0.474 mmol) dissolved in dry DMF them 1eq of DIPEA was added. After 30 min [Reactants] and 1 eq of DIPEA were added in raw. The reaction was stirred at r.t. until the starting compound consumed (UPLC monitoring approximately 2 hours). After the reaction finished, the solvent was evaporated via rotary evaporation. The crude was diluted with 10 mL CH_2Cl_2 and washed with 1 mL 1 M HCl and 5 mL water. After extraction, the organic layer was dried over sodium sulfate and CH_2Cl_2 was evaporated under reduced pressure via rotavap. The crude purified with flash chromatography (0-10 % MeOH/ CH_2Cl_2). [Products] was obtained as colorless oil. After lyophilization the color turned to white solid.

^{1}H NMR (400 MHz, DMSO-d_6, δ): 2.89 (m, 2H), 4.24 (m, 8H), 4.49 (m, 1H), 4.61 (m, 1H), 5.15 (d, J = 8.6 Hz, 1H), 7.75 (d, J = 9.4 Hz, 1H), 7.88 (d, J = 4.8 Hz, 1H), 8.03 (s, 1H), 8.34 (d, J = 9.2 Hz, 1H), 9.07 (d, J = 4.6 Hz, 1H), 9.43 (t, J = 5.7 Hz, 1H). **^{13}C NMR** (100 MHz, DMSO-d_6, δ), 36.5 (t, $J_{C\text{-}T}$ 25), 41.4, 44.3 (d, $J_{C\text{-}T}$ 7), 48.6, 51.2 (t, $J_{C\text{-}T}$ 32), 61.9, 73.1 (dd, $J_{C\text{-}T}$ 4, 19), 69.4 (d, $J_{C\text{-}T}$ 8), 82.6 (dd, $J_{C\text{-}T}$ 11, 167), 105.1, 117.8, 119.9, 125.9, 126.9 (t, $J_{C\text{-}T}$ 250), 137.8, 143.9, 146.1, 158.3, 165.8, 167.5. **MS** t_R 1.16 min. UPLC MS (ESI) m/z 543.3 $[M+Na]^+$, m/z 435.2 $[M-H]^-$, m/z 481.3 $[M+FA-H]^-$. HRMS(ESI) $C_{20}H_{18}F_3N_4O_4$ $[M-H]^-$, calcd 435.1286; found 435.1290

Methyl 6-((*trans*-2,2-dimethyl-5-((tosyloxy)methyl)-1,3-dioxolan-4-yl)methoxy)quinoline-4-carboxylate (26)

A 10 mL round bottom flask was charged with methyl 6-hydroxyquinoline-4-carboxylate (0.4g, 1.969 mmol), Cesium carbonate (3.21 g, 9.84 mmol) and 10 mL of dry DMF. After 15 min stirring at 40 ℃ ((*trans*)-2,2-dimethyl-1,3-dioxolane-4,5-diyl)bis(methylene) bis(4-methylbenzenesulfonate) (1.2 eq) was added to the mixture at room temparature and the

reaction was heated up again to 40 ℃. After the starting materials were consumed (UPLC monitoring), the reaction was quenched with slush and extracted with EtOAc (3 x 10 mL). The combined organic layers were washed with brine (3 x 5 ml) and dried over Na_2SO_4. The water-saturated Na_2SO_4 was filtered off and the solvent was eliminated under reduced pressure to give a residue that was purified by silica gel column chromatography. The title compound was obtained by eluting with 5-50 % EtOAc / *n*-heptane and obtained as a white solid (31 % yield). **^{1}H NMR** (400 MHz, DMSO-d_6, δ): 1.33 (d, *J* = 18.2 Hz, 6H), 2.35 (s, 3H), 3.98 (s, 3H), 4.22 (m, 5H), 4.37 (d, *J* = 9.4 Hz, 1H), 7.44 (dd, *J* = 2.9, 9.2 Hz, 1H), 7.45 (d, *J* = 8.5 Hz, 2H), 7.81 (d, *J* = 8.3 Hz, 2H), 8.94 (d, *J* = 4.4 Hz, 1H), 8.03 (d, *J* = 3.4 Hz, 1H), 8.05 (d, *J* = 9.4 Hz, 1H), 8.90 (d, *J* = 4.3 Hz, 1H). **^{13}C NMR** (100 MHz, DMSO-d_6, δ), 21.1, 26.7, 26.8, 52.8, 67.8, 69.8, 74.6, 75.2, 104.3, 109.8, 122.2, 122.7, 125.5, 127.7, 130.17, 131.4, 132.1, 132.7, 144.9, 145.1, 147.7, 157.4, 166.3. **MS** t_R 2.11 min, UPLC MS (ESI) m/z 502.2 $[M+H]^+$, m/z 524.1 $[M+Na]^+$.

6-((*trans*-2,2-Dimethyl-5-((tosyloxy)methyl)-1,3-dioxolan-4-yl)methoxy)quinoline-4-carboxylic acid (27)

A 10 mL cylindrical flask was charged with methyl 6-(((*trans*)-2,2-dimethyl-5-((tosyloxy)methyl)-1,3-dioxolan-4-yl)methoxy)quinoline-4-carboxylate (0.24 g, 0.479 mmol) and 5 mL of dry MeOH. Afterwards, NaOH (5 eq) was added and stirred at 40 ℃ until the starting compound was consumed (UPLC monitoring). Subsequently, 0.5 mL of EtOAc was added to the mixture and the pH of the reaction mixture was adjusted to 6 by adding the neccesary amount of 1 M HCl at room temperature. The formed precipitate was collected by filtration through a glass filter and dried under high vacuum. The title compound was obtained as white solid (quantitative yield). **^{1}H NMR** (400 MHz, DMSO-d_6, δ): 1.33 (d, *J* = 17.9 Hz, 6H), 2.35 (s, 3H), 4.19 (m, 5H), 4.36 (d, *J* = 8.7 Hz, 1H), 7.40 (dd, *J* = 2.9, 9.2 Hz, 1H), 7.46 (d, *J* = 7.9

Hz, 2H), 7.81 (d, *J* = 8.3 Hz, 2H), 7.91 (d, *J* = 4.4 Hz, 1H), 8.02 (d, *J* = 9.1 Hz, 1H), 8.13 (d, *J* = 2.6 Hz, 1H), 8.87 (d, *J* = 4.4 Hz, 1H). **^{13}C NMR** (100 MHz, DMSO-d_6, δ), 21.5, 27.1, 27.3, 68.3, 70.28, 75.1, 75.7, 105.3, 110.2, 122.3, 123.0, 126.3, 128.2, 130.6, 131.7, 132.6, 145.4, 145.6, 148.3, 157.5, 168.1. **MS** t_R 1.57 min, UPLC MS (ESI) m/z 488.2 $[M+H]^+$ (92%).

((*trans*)-5-(((4-((2-((*S*)-2-Cyano-4,4-difluoropyrrolidin-1-yl)-2-oxoethyl)carbamoyl)quinolin-6-yl)oxy)methyl)-2,2-dimethyl-1,3-dioxolan-4-yl)methyl 4-methylbenzenesulfonate (28)

The compound was prepared according to General procedure A using 6-(((*trans*)-2,2-dimethyl-5-((tosyloxy)methyl)-1,3-dioxolan-4-yl)methoxy)quinoline-4-carboxylic acid (0.21 g, 0.431 mmol) and (*S*)-2-(2-cyano-4,4-difluoropyrrolidin-1-yl)-2-oxoethan-1-aminium 4-methylbenzene sulfonate (1.1 eq) as reactants. After purification of the residue by silica gel column chromatography, the title compound was eluted with 0-6 % MeOH / dichloromethane and obtained as a white solid (20 % yield**). ^{1}H NMR** (400 MHz, DMSO-d_6, δ): 1.30 (s, 3H), 1.34 (s, 3H), 2.33 (s, 3H), 2.90 (m, 2H), 4.25 (m, 10H), 5.11 (dd, *J* = 2.7, 9.3 Hz, 1H), 7.41 (dd, *J* = 2.7, 9.4 Hz, 1H), 7.45 (d, *J* = 8.0 Hz, 2H), 7.52 (d, *J* = 4.1 Hz, 1H), 7.81 (d, *J* = 8.3 Hz, 2H), 7.86 (d, *J* = 2.7 Hz, 1H), 8.00 (d, *J* = 9.1 Hz, 1H), 8.83 (d, *J* = 4.3 Hz, 1H), 9.11 (t, *J* = 6.3 Hz, 1H). **^{13}C NMR** (100 MHz, DMSO-d_6, δ), 21.0, 26.7, 26.8, 36.3 (t, J_{C-T} 23), 41.3, 44.1, 44.2, 51.2 (t, J_{C-T} 32), 68.4, 69.6, 74.8, 75.1, 104.6, 109.8, 117.8, 119.3, 122.3, 125.3, 127.7, 130.2, 130.8, 132.1, 140.9, 144.2, 145.1, 147.2, 156.6, 167.5, 168.2. **MS t_R** 2.04 min. UPLC MS (ESI) m/z 659.3 $[M+H]^+$, m/z 681.3 $[M+Na]^+$.

6-(((*trans*)-5-(Fluoromethyl)-2,2-dimethyl-1,3-dioxolan-4-yl)methoxy)quinoline-4-carboxylic acid (29)

A 10 mL cylindrical flask was charged with methyl 6-(((*trans*)-2,2-dimethyl-5-((tosyloxy)methyl)-1,3-dioxolan-4-yl)methoxy)quinoline-4-carboxylate (0.15 g, 0.299 mmol), 2

mL of acetonitrile and tetrabutylammonium fluoride (5 eq). The reaction was stirred at 80 ºC until consumption of starting compound (UPLC monitoring). Afterwards, all volatiles were evaporated and the crude was diluted with 5 mL of CH_2Cl_2. It was washed with H_2O (5 x 2mL) and dried over Na_2SO_4, filtered and the solvent was eliminated under reduced pressure. The obtained residue was purified by silica gel column chromatography, eluting the target molecule with 0-6 % MeOH / dichloromethane and obtaining it as a yellow solid (40 % yield). **^{1}H NMR** (400 MHz, DMSO-d_6, δ): 1.39 (d, *J* = 10.4 Hz, 6H), 4.32 (m, 4H), 4.65 (t, *J* = 46.9 Hz, 2H), 7.55 (d, *J* = 8.4 Hz, 1H), 7.94 (s, 1H), 8.04 (d, *J* = 9.2 Hz, 1H), 8.19 (s, 1H), 8.88 (s, 1H), 13.79 (brs, 1H). **^{13}C NMR** (100 MHz, DMSO-d_6, δ), 26.8, 26.9, 68.2, 74.0 (d, $J_{C\text{-}T}$ 7), 76.3 (d, $J_{C\text{-}T}$ 18), 81.6 (d, $J_{C\text{-}T}$ 169), 104.7, 109.7, 122.12, 122.7, 125.8, 131.3, 134.1, 144.9, 147.8, 157.3, 167.6. **MS** t_R 1.17 min. UPLC MS (ESI) m/z 336.1 $[M+H]^+$.

***N*-(2-((*S*)-2-Cyano-4,4-difluoropyrrolidin-1-yl)-2-oxoethyl)-6-(((*trans*)-5-(fluoromethyl)-2,2-dimethyl-1,3-dioxolan-4-yl)methoxy)quinoline-4-carboxamide (30)**

The title compound was prepared according to **General procedure A** using 6-(((*trans*)-5-(fluoromethyl)-2,2-dimethyl-1,3-dioxolan-4-yl)methoxy)quinoline-4-carboxylic acid (0.04 g, 0.119 mmol) and (*S*)-2-(2-cyano-4,4-difluoropyrrolidin-1-yl)-2-oxoethan-1-aminium 4-methylbenzenesulfonate (1.1 eq) as reactants. After purification of the residue by silica gel column chromatography eluting with 0-10 % MeOH / dichloromethane, the title compound was obtained as a white solid (16 % yield). **^{1}H NMR** (400 MHz, DMSO-d_6, δ): 1.38 (s, 3H), 1.40 (s, 3H), 2.89 (m, 2H), 4.23 (m, 8H), 4.65 (m, 2H), 5.13 (dd, *J* = 2.5, 9.3 Hz, 1H), 7.51 (m, 2H), 7.93 (d, *J* = 2.6 Hz, 2H), 8.00 (d, *J* = 9.2 Hz, 1H), 8.82 (d, *J* = 4.4 Hz, 2H), 9.32 (t, *J* = 6.3 Hz, 1H). **^{13}C NMR** (100 MHz, DMSO-d_6, δ), 26.8, 26.9, 41.32, 44.1, 44.2, 68.6, 74.2, 74.3, 76.0, 76.2, 81.5,

83.2, 104.7, 109.7, 117.7, 119.2, 122.4, 125.3, 130.8, 141.0, 144.2, 147.7, 156.7, 167.5, 168.2. **MS** t_R 1.50 min. UPLC MS (ESI) m/z 505.3 $[M-H]^-$, m/z 551.3 $[M+FA-H]^-$.

_N_-(2-((_S_)-2-Cyano-4,4-difluoropyrrolidin-1-yl)-2-oxoethyl)-6-((_trans_)-4-fluoro-2,3-dihydroxybutoxy)quinoline-4-carboxamide (31)

A 5 mL cylindrical flask was charged with methyl *N*-(2-((*S*)-2-cyano-4,4-difluoropyrrolidin-1-yl)-2-oxoethyl)-6-((*trans*)-4-fluoro-2,3-dihydroxybutoxy)quinoline-4-carboxamide (10 mg, 0.214 mmol), 2 mL MeOH and 0.5 mL 2 M HCl in diethyl ether. The reaction was stirred at room temperature until consumption of the starting compound (UPLC monitoring). Afterwards, all volatiles were evaporated and the crude was washed with heptane (3 x 2mL). The solvent was eliminated under reduced pressure to afford the title compound obtained as white solid (50 % yield). **^{1}H NMR** (400 MHz, DMSO-d_6, δ): 2.93 (m, 2H), 3.9 (m, 2H), 4.25 (m, 4H), 4.52 (m, 2H) 5.12 (d, *J* = 9.6 Hz, 1H), 7.7 (m, 2H), 7.78 (d, *J* = 2.4 Hz, 2H), 8.0 (d, *J* = 9.6 Hz, 1H), 8.84 (d, *J* = 5 Hz, 2H), 9.16 (t, *J* = 6.3 Hz, 1H). **^{13}C NMR** (100 MHz, DMSO-d_6, δ): 36.8 (t, J= 25 Hz), 41.6, 45.7, 51.8 (t, J= 24 Hz), 69.5 (d, *J* = 8 Hz), 69.7, 84.9 (d, *J*= 165 Hz), 103.3, 104.9, 109.7, 118.2, 119.9, 120.8, 126.0, 130.6, 141.0, 150.2, 157.7, 166.4, 167.8. HRMS(ESI) $C_{21}H_{22}F_3N_4O_5$ $[M+H]^+$, calcd 467.1537; found 467.1540

6-(3-Chloropropoxy)quinoline-4-carboxylic acid (32)

In a round-bottom flask, 1-bromo-3-chloropropane (5.23 ml, 52.9 mmol) was added to a suspension of 6-hydroxyquinoline-4-carboxylic acid (2.5 g, 13.22 mmol) and cesium carbonate (43.1 g, 132 mmol) and the mixture was stirred at 60°C overnight. The mixture was then filtered under vacuum and the solids were washed with EtOAc. The filtrate was collected and partially evaporated to reduce its volume. It was then diluted with 50mL of CH_2Cl_2, and washed

with 25mL of cold water. The water fraction was back-extracted once with 25mL of dichloromethane and the combined organic fractions were evaporated under reduced pressure. The obtained residue was diluted with 25mL of water and 50mL of acetonitrile, then 10mL of NaOH 6M were added and the mixture was stirred until complete hydrolysis of the ester. The mixture spontaneously separated into a top organic layer and a bottom aqueous layer. The water layer was set aside and the organic layer was evaporated under reduced pressure. The residue was redissolved in 25mL of CH_2Cl_2 and extracted with 25mL of water. The aqueous phase was washed once with 25mL of diethyl ether and subsequently titrated with HCl 6M to pH 5, forming a milky beige precipitate, that was collected with a glass filter and dried under reduced pressure to obtain 6-(3-chloropropoxy)quinoline-4-carboxylic acid (2.289 mg, 8,62 mmol, 65,2 % yield). **^{1}H NMR** (400 MHz, DMSO) δ 2.27 (p, *J* = 6.2 Hz, 2H 8.87), 3.86 (t, *J* = 6.5 Hz, 2H), 4.24 (t, *J* = 6.0 Hz, 2H), (d, *J* = 4.4 Hz, 1H), 7.52 (dd, *J* = 9.2, 2.7 Hz, 1H), 7.93 (d, *J* = 4.4 Hz, 1H), 8.03 (d, *J* = 9.2 Hz, 1H), 8.19 (d, *J* = 2.8 Hz, 1H). **UPLC MS** (ESI): m/z 266.0 $[M+H]^+$ (^{35}Cl); 268.0 $[M+H]^+$ (^{37}Cl).

6-(3-(Dimethylamino)propoxy)quinoline-4-carboxylic acid (33)

A suspension of 6-(3-chloropropoxy)quinoline-4-carboxylic acid (768 mg, 2.312 mmol), Potassium iodide (38.4 mg, 0.231 mmol), and dimethylamine 2M solution in THF (11.562 mL, 23.12 mmol) were stirred at 60°C overnight in a pressure tube. 2 Eq of NaOH 6 M were added and the solvent was then removed via rotary evaporator and the obtained product was used in the following reaction without further purification. **UPLC MS** (ESI): m/z=275.1 $[M+H]^+$

(*S*)-*N*-(2-(2-Cyano-4,4-difluoropyrrolidin-1-yl)-2-oxoethyl)-6-(3-(dimethylamino)propoxy) quinoline-4-carboxamide (34)

A round bottom flask was charged with 6-(3-(dimethylamino)propoxy)quinoline-4-carboxylic acid (642 mg, 2.340 mmol), HATU (1068 mg, 2.81 mmol), and dry DIPEA (2.038 mL, 11.70 mmol) in dry DMF (23 mL). After 5' stirring at room temperature, (*S*)-2-(2-cyano-4,4-difluoropyrrolidin-1-yl)-2-oxoethan-1-aminium 4-methylbenzenesulfonate (1015 mg, 2.81 mmol) was added and the reaction was stirred until consumption of the starting material (checked via UPLC, about 2h). The crude mixture was diluted with 200mL of EtOAc and washed with 3x40mL of saturated sodium bicarbonate solution and 30mL of brine and evaporated via rotary evaporator. The obtained crude was purified via reverse-phase flash chromatography with a gradient of water/ACN. The product was further purified via RP-HPLC with a gradient of ACN in Water + 0.1% formic acid (5-50% in 20'). (4% yield). **^{1}H NMR** (400 MHz, DMSO) δ 2.16 (p, *J* = 7.8 Hz, 2H), 2.92 (m, 2H), 2.75 (s, 6H), 3.17 (m, 2H), 4.15 (m, 1H), 4.21 (d, *J* = 6.0 Hz, 2H), 4.24 (d, *J* = 6.3 Hz, 2H), 4.34 (m, 1H), 5.15 (dd, *J* = 9.3, 3.0 Hz, 1H), 7.47 (dd, *J* = 9.2, 2.8 Hz, 1H), 7.54 (d, *J* = 4.3 Hz, 1H), 7.89 (d, *J* = 2.8 Hz, 1H), 8.01 (d, *J* = 9.2 Hz, 1H), 8.83 (d, *J* = 4.3 Hz, 1H), 9.13 (t, *J* = 6.0 Hz, 1H). **UPLC MS** (ESI): m/z=223.7 $[M+2H]^{++}$; 446.3 $[M+H]^{+}$; 468.2 $[M+Na]^{+}$.

(*S*)-3-((4-((2-(2-cyano-4,4-difluoropyrrolidin-1-yl)-2-oxoethyl)carbamoyl)quinolin-6-yl)oxy)-*N*-(fluoromethyl)-N,N-dimethylpropan-1-aminium benzenesulfonate (35)

(*S*)-*N*-(2-(2-cyano-4,4-difluoropyrrolidin-1-yl)-2-oxoethyl)-6-(3-(dimethylamino)propoxy) quinoline-4-carboxamide (30 mg, 0.067 mmol) was dissolved in DMF (168 µl) in a glass vial. fluoromethyl 4-methylbenzenesulfonate (68.8 µl, 0.337 mmol) and DIPEA (58.7 µl, 0.337 mmol) were added and the reaction was stirred at 120°C for 20'. The solvent was removed under reduced pressure and the crude mixture was purified via preparative HPLC. (47 % yield).

^{1}H NMR (400 MHz, MeOD) δ 2.33 (s, 3H), 2.41 (p, *J* = 5.1 Hz, 2H), 2.89 (m, 2H), 3.22 (m, 6H), 3.70 (dd, *J* = 10.6, 6.1 Hz, 2H), 4.12 (m, 1H), 4.25 (m, 1H), 4.32 (s, 2H), 4.37 (t, *J* = 5.9 Hz, 2H), 5.15 (dd, *J* = 9.4, 3.3 Hz, 1H), 5.46 (d, *J* = 13.7 Hz, 2H), 7.21 (d, *J* = 7.9 Hz, 2H), 7.47 (dd, *J* = 9.2, 2.8 Hz, 1H), 7.57 (d, *J* = 4.4 Hz, 1H), 7.68 (d, *J* = 8.1 Hz, 2H), 7.99 (d, *J* = 9.3 Hz, 1H), 8.04 (d, *J* = 2.7 Hz, 1H), 8.77 (d, *J* = 4.4 Hz, 1H). **^{13}C NMR** (100 MHz, MeOD) δ 21.3, 23.3, 37.9 (t, *J* = 25.1 Hz), 42.9, 45.9 (d, *J* = 5.7 Hz), 48.0, 52.9 (t, *J* = 32.3 Hz), 60.6, 66.3, 96.6, 98.8, 105.7, 118.5, 120.3, 124.6, 129.9, 131.1, 141.7, 143.0, 143.6, 145.4, 148.4, 158.7, 169.7, 170.6, 127.2. **UPLC MS** (ESI): m/z=239.7 $[M+H]^{2+}$; 478.3 $[M]^{+}$ HRMS(ESI) $C_{23}H_{27}F_3N_5O_3$ $[M]^{+}$, calcd 478.2061; found 478.2096

Biochemistry. For the biochemical evaluation, the same procedures were followed as described in Benramdane *et al*.[35] DPP4 was purified from human seminal plasma as described previously.[36] Recombinant human (rh) DPP8 and rhDPP9 were expressed in Sf9 insect cells using the *N*-terminal BaculoDirect insect cell expression system (Invitrogen) and were purified as described by De Decker *et al*.[37] rhDPP2 was purchased from R&D (3438-SE). rhFAP (extracellular domain, amino acid 27-760) with a C-terminal His-tag was expressed and purified in Sf9 insect cells as described before. rhPREP was expressed in BL21(DE3) cells and purified as described by De Decker *et al*.[37]

Radiochemistry. All radiofluorinations were performed on a fully automated TRASIS AllinOne module (TRASIS). No-carrier added aqueous [^{18}F]fluoride ([^{18}F]F^{-}) was produced in an Eclipse HP cyclotron (Siemens) using the $^{18}O(p,n)^{18}F$ reaction by proton bombardment of [^{18}O]H_2O (Rotem Industries). After transferring to the hot cell, [^{18}F]fluoride was isolated from enriched water by trapping in a silica-based anion exchange cartridge (QMA, Waters), previously conditioned with potassium bicarbonate solution (0.25 g/5 ml) and water (10 ml).

***N*-(2-((*S*)-2-cyano-4,4-difluoropyrrolidin-1-yl)-2-oxoethyl)-6-(3-(fluoro-^{18}F)-2-methoxypropoxy)quinoline-4-carboxamide (7)**

After washing the QMA with 3 mL anhydrous acetonitrile, a N_2 flow was passed through the column for 10 min. [^{18}F]fluoride was eluted from the column in the reverse direction using 38 mM TEAB in DMSO/H_2O (90 : 10 v/v) into the reaction vial. The tosylated precursor dissolved in 500 µL anhydrous DMSO was then added to the [^{18}F]F^- solution and the reaction vial was heated to 105 °C for 10 min. The reaction mixture was cooled to 40°C and diluted with 1 mL H_2O, passed through a Sep-Pak Alumina N Light cartridge (Waters) (preconditioned with 10 mL of water), before injection onto a semi-preparative HPLC column (Phenomenex Luna C18 250 × 10 mm (5 µm), EtOH/50 mM Na acetate pH 5.5 30 : 70 (v/v), 3 mL min^{-1} flow rate). The product was collected (t_R = 23 min), sterile-filtered and diluted with 0.9% NaCl solution to reduce ethanol concentration to < 10% in the final formulation. The total synthesis time was 60 min.

***N*-(2-((*S*)-2-cyano-4,4-difluoropyrrolidin-1-yl)-2-oxoethyl)-6-(3-(fluoro-^{18}F)-2-hydroxypropoxy)quinoline-4-carboxamide (8)**

[^{18}F]fluoride was eluted from the QMA cartridge to reaction vial 1 with 0.8 mL of a 38 mM TEAB solution in ACN/H_2O (90 : 10 v/v) and evaporated to complete dryness. After cooling to 50°C, the tosylated precursor dissolved in 500 µL anhydrous DMSO was then added to the dried [^{18}F]F^- and the reaction vial was heated to 110°C for 10 min. Next, the reaction mixture was cooled to 50°C and quenched with WFI (3 mL), passed through a Sep-Pak Alumina N Light cartridge (Waters) (preconditioned with 10 mL of water), and loaded on a Sep-Pak tC18 cartridge (Waters). After washing with 3 mL of water, the cartridge was eluted to a second reaction vial using 3 mL MeOH, where the product was deprotected with a 0.3 mL 4 N HCl

solution in dioxane for 2 min at room temperature. The crude reaction mixture was neutralized with 2.5 mL 0.5 M phosphate buffer (pH 12) before injection onto a semi-preparative HPLC column (Waters XBridge C18 OBD 150 × 10 mm (5 µm), EtOH/50 mM Na acetate pH 5.5 15 : 85 (v/v), 2 mL min^{-1} flow rate). The product was collected (t_R = 20 min), sterile-filtered and diluted with 0.9% NaCl solution to reduce ethanol concentration to < 10% in the final formulation. The total synthesis time was 60 min.

***N*-(2-((*S*)-2-cyano-4,4-difluoropyrrolidin-1-yl)-2-oxoethyl)-6-(4-(fluoro-^{18}F)-2,3-dihydroxybutoxy)quinoline-4-carboxamide (9)**

[^{18}F]fluoride was eluted from the QMA cartridge to reaction vial 1 with 0.8 mL of a 38 mM TEAB solution in MeCN/H_2O (90 : 10 v/v) and evaporated to complete dryness. After cooling to 50°C, the tosylated precursor dissolved in 500 µL anhydrous DMSO was then added to the dried [^{18}F]F^- and the reaction vial was heated to 110°C for 9 min. Next, the reaction mixture was cooled to 50°C and quenched with WFI (3 mL), passed through a Sep-Pak Alumina N Light cartridge (Waters) (preconditioned with 10 mL of water), and loaded on a Sep-Pak tC18 cartridge (Waters). After washing with 3 mL of water, the cartridge was eluted to a second reaction vial using 3 mL MeOH, where the product was deprotected with a 0.6 mL 4N HCl solution in dioxane for 3 min at 40°C. The crude reaction mixture was neutralized with 2.5 mL 0.7 M phosphate buffer (pH 12) before injection onto a semi-preparative HPLC column (Waters XBridge C18 OBD 250 × 10 mm (5 µm), EtOH/50 mM Na acetate pH 5.5 15 : 85 (v/v), 3 mL min^{-1} flow rate). The product was collected (t_R = 25 min), sterile-filtered and diluted with 0.9% NaCl solution to reduce ethanol concentration to < 10% in the final formulation. The total synthesis time was 60 min.

(*S*)-3-((4-((2-(2-cyano-4,4-difluoropyrrolidin-1-yl)-2-oxoethyl)carbamoyl)quinolin-6-yl)oxy)-*N*-((fluoro-^{18}F)methyl-*d2*)-*N*,*N*-dimethylpropan-1-aminium (10)

[^{18}F]fluoride was eluted from the cartridge to reaction vial 1 with 0.8 mL of a mixture of 0.03 M K_2CO_3/0.07 M Kryptofix 222 in MeCN/H_2O (95 : 5 v/v) and evaporated to complete dryness. The thoroughly dried [^{18}F]F^- was cooled to 40°C and dibromomethane-d2 (500 µL) in 500 µL anhydrous ACN was added to reaction vial 1. The mixture was heated to 90 °C for 5 min. After cooling reactor 1 to 40 °C, purification of [^{18}F]FCD_2Br was performed by distillation over 3 silica plus SepPak® cartridges using a smooth He stream (1 min with 10 mL/min; then 40 mL/min for 10-15 min) and the pure [^{18}F]FCD_2Br was trapped in reactor 2 and subsequently reacted with precursor (4 mg in 400 µL anhydrous DMF) in the presence of NaOH. The alkylation reaction was performed for 10 min at 100 °C. The reaction mixture was cooled to 40°C and quenched by addition of 1 mL HPLC buffer (MeCN/0.05M TEA acetate pH 5.0 20 : 80 (v/v)). The crude solution was purified by semi-preparative HPLC (SIELC Primesep C 150 × 10 mm (5 µm) HPLC column, ACN/0.05M TEA acetate pH 5.0 (20 : 80 v/v); 4 mL min^{-1} flow rate). The fraction containing **10** (t_R = 30 min) was collected, and evaporated. The radiotracer was diluted with a 0.9% NaCl/ethanol solution to obtain a formulation containing < 10% EtOH. The total synthesis time was 90 min.

Radiosynthesis of [^{68}Ga]Ga-DATA^{5m}-SA-FAPi and [^{68}Ga]Ga-DOTA-FAPI-04

Gallium-68 was obtained from a ^{68}Ge/^{68}Ga-generator (Galli Ad^{TM}, IRE ELiT) by elution with 0.1N HCl. The radiolabeling reaction was performed with incubation of the [^{68}Ga]Ga^{3+} eluate with the respective precursor (19 µg DATA^{5m}.SA.FAPi or 25 µg DOTA-FAPI-04) at room temperature or 95°C in ammonium acetate buffer (1 M, pH 4.7-5.5) for 10 or 20 min, respectively. After radiolabeling the ^{68}Ga-labelled compounds were purified by solid-phase extraction (Sep-Pak

Light C18 cartridge, Waters) to remove uncomplexed gallium-68, and formulated in 0.9% NaCl with 5% ethanol.

HPLC method for quality control of 7,8,9 and 10. Quality control of the radiotracers was performed using analytical radio-HPLC and a Shimadzu LC-20AT HPLC equipped with an SPD-20A UV/VIS detector (λ = 250 nm) in series with a NaI-scintillation detector for radiation detection (Raytest). HPLC column and method: Waters XBridge C18 150 × 4.6 mm (5 µm) HPLC column. Gradient method: 10 to 90% ACN + 0.1% TFA in H_2O + 0.1% TFA over 20 min, with a flow rate of 1 mL min^{-1}. The recorded data were processed by the GINA-Star 5 software (Raytest).

Quality control methods for [^{68}Ga]Ga-DATA^{5m}.SA.FAPi and [^{68}Ga]Ga-DOTA-FAPI-04. HPLC column and method: Phenomenex Luna C18 250 × 4.6 mm (5 µm) HPLC column. Gradient method: 5 to 95% ACN + 0.1% TFA in H_2O + 0.1% TFA over 10 or 15 min, with a flow rate of 1 mL min^{-1}. Radiochemical purity was also assessed using radio-TLC (TLC Silica gel 60F254, Merck) with citrate buffer pH 4.0. The labeled complexes were observed at a Rf value of 0.1-0.2, and free radiometal at a Rf value of 0.8-0.9.

All the radiotracer formulations were sterile filtered. The pH of the formulations was between pH 6 and 8. Radiochemical purity was determined by analytical reverse-phase HPLC using gradient methods as mentioned above. Radiochemical yields (RCY) were calculated from the theoretical initial amount of [^{18}F]F^- and decay corrected to end of bombardment (EOB).

Determination of LogD. The partition coefficient (logD) of the radiotracers was measured using the 'shake-flask' method. Briefly, approximately 74 kBq of a radiotracer was added to a test tube containing a mixture of 2 mL n-octanol and 2 mL PBS (0.01 M, pH 7.4). The mixture was shaken well, vortexed for 2 min and centrifuged at 3,000 rpm for 10 min. After separation

of the layers, a 0.5 mL aliquot of both layers was taken into separate tubes and counted for radioactivity in an automatic gamma- (γ) counter (Wizard^2 2480, PerkinElmer). Corrections were made for differences in mass and density between the two phases. The octanol-water partition coefficients were obtained by dividing the octanol containing radioactivity by the PBS containing radioactivity and the $\log_{10}$ of this ratio was calculated.

***In vivo* experiments: Biodistribution, Stability determination, PET imaging.** All experiments were approved by the Ethics Committee of the University of Antwerp, Belgium (file number 2021-01). The use of laboratory rodents was carried out in strict accordance with all mandatory guidelines (EU directives, including the Revised Directive 2010/63/EU on the Protection of Animals used for Scientific Purposes that came into force on 01/01/2013, and the declaration of Helsinki in its latest version).

Biodistribution studies using control mice. Six- to eight-week-old female CD1$^{-/-}$ nude mice (body weight, 20–25 g; Charles River Laboratories) were injected with 5.1 - 7.4 MBq of the radiotracer via the lateral tail vein. At 15, 30, 60 (n = 3 for each time point) post-radiotracer injection (p.i.) the blood was collected through cardiac puncture and the mice were euthanized by cervical dislocation. The organs and tissues were harvested, weighed and the radioactivity in the samples was measured using an automatic γ-counter. The uptake levels of the tracers in the organs and tissues were expressed as percentage of the injected dose per gram (%ID g^{-1}).

Ex vivo metabolite analysis. The blood from the above *ex vivo* biodistribution studies was collected in EDTA-coated tubes and used to evaluate the *in vivo* plasma stability of the radiotracers (n = 3 per time point) using the procedure described hereafter.

In vitro stability evaluation. The recovery of the radiotracers, and their stability during the work-up were first determined in control experiments using blood spiked *in vitro* with 185 kBq of the corresponding tracer. Sample work-up was performed as follows. The plasma fraction was obtained by centrifugation at 4,000 *g* for 7 min, and mixed (200 µL) with an equal volume of cold ACN, followed by vortexing and centrifugation (4 min, 4,000 *g*) to enable sample deproteination. The supernatant and the pellet were γ-counted separately to determine the amount of recovered radioactivity in the organic phase. The radioactive contents of the supernatant were analyzed by analytical radio-HPLC. The HPLC eluate was collected in fractions of 30s, and the radioactivity was counted in an automatic γ-counter. The stability of the radiotracers was evaluated in PBS (0.01 M, pH 7.4) and in mouse plasma at 37 °C for up to 60 min using the same procedure described above. All experiments were performed in triplicate.

In vivo tumor model. The xenograft models were generated by subcutaneous injection of HT29 (10×10^6, n=4; ATCC HTB-38) or U-87MG (5×10^6, n=4; ATCC HTB-14) cells, both in in 100 µL of Dulbecco phosphate-buffered saline, into the hind flank of 6- to 8-wk-old female $CD1^{-/-}$ nude mice (body weight, 20–25 g; Charles River Laboratories). When xenografts reached approximately 200 mm^3, mice underwent PET/CT scanning.

In vivo small-animal PET imaging studies. For *in vivo* PET imaging studies, normal (n = 3) or tumor-bearing $CD1^{-/-}$ nude mice (n = 8) were anesthetized using isoflurane (5% for induction, 2% for maintenance), placed on the animal bed in the scanner and injected via lateral tail vein catheterization with 5-7.4 MBq of the corresponding radiotracer. To confirm the binding specificity of each radiotracer, a cohort of tumor-bearing mice (n=4) was injected via the tail vein with UAMC1110 (compound **1, Figure 1**) 30 min before radiotracer injection.

Dynamic whole-body PET images were acquired during 60 min (12×10s, 3×20s, 3×30s, 3×60s, 3×150s and 9×300s frames) using an Inveon small-animal PET/CT scanner (Siemens). Following each PET acquisition, a whole-body CT scan was acquired to obtain anatomic information for segmentation. Throughout the entire PET/CT scanning procedure, the mice were maintained at constant body temperature by using a heating pad. For quantitative analysis, PET data were reconstructed using a list-mode iterative reconstruction with proprietary spatially variant resolution modeling in 8 (for ^{18}F) or 16 (for ^{68}Ga) iterations and 16 subsets of the 3D ordered subset expectation maximization (OSEM 3D) algorithm(5). Normalization, dead time, and CT-based attenuation corrections were applied. The PET images were additionally reconstructed on a 128 × 128 × 159 matrix with a voxel size of 0.776 × 0.776 × 0.776 mm. CT-based attenuation and single scatter stimulation (SSS) scatter corrections were applied to the PET data. Volumes of interest (VOIs) were manually drawn on the PET/CT images using PMOD (version 3.6; PMOD Technologies) to delineate the tumor regions and muscle, as a reference background region. Tumor and muscle delineation were carefully performed on the CT images avoiding bone structures. The average tumor or muscle activity per volume was obtained from the co-registered PET images and the decay-corrected time-activity curves (TACs) were extracted. For an absolute measure of tracer uptake, normalized images were scaled according to the percent injected dose (%ID mL^{-1} = tissue uptake [kBq mL^{-1}]/injected dose [kBq] × 100).

Autoradiography. After γ-counting, the tumors were immediately snap-frozen, embedded in OCT compound (VWR), sectioned (100 µm), and exposed to phosphor screen plates (Fujifilm) overnight. Exposed plates were imaged in a Phosphor Imager system (FLA7000; GE Healthcare) for visualization of regional tracer distribution in the tumors.

***Ex vivo* immunohistochemistry.** Adjacent tumor sections (10 μm) were taken at regular intervals across the entire tumor volume and used for immunohistochemical analysis of FAP expression in the tumor xenografts. The cryosections were thawed and the tumor sections were delineated with an IHC PAP pen (DAKO). The sections were washed 2 times for 5 minutes with DPBS, followed by 10 minutes fixation with 4% paraformaldehyde (PFA). Subsequently, sections were permeabilized with 0.1% Triton X-100 in 2% goat serum in DPBS. Blocking was performed for 30 minutes using 2% goat serum in DPBS followed by three washes of 5 minutes with DPBS. Fixation, permeabilization, blocking and washing steps were all carried out at room temperature. The sections were incubated with the primary anti-FAP antibody (1:100 dilution in 2% goat serum; R&D; cat. No. AF3715) and anti-αSMA antibody (1:200 in 2% goat serum; Invitrogen; cat. No. 14-9760-82) overnight at 4 °C. After three washing steps with DPBS, the cryosections were incubated for 1 hour at room temperature with donkey-anti-sheep-Alexa Fluor 594 and Goat-anti-mouse Alexa Fluor 488 (1:200 in 2% goat serum). Next, the slides were mounted using Vectashield antifade mounting medium with DAPI (Vector lab, H-1200) and images were acquired using an inverted Leica TCS SP8 confocal laser scanning microscope.

Quantification of FAP expression was performed in 12 randomly selected tumor images collected across three non-sequential tumor sections (four tumors were evaluated per radiotracer). Images were acquired using identical fluorescence excitation and detection settings to avoid channel crosstalk. Image analysis of FAP quantification was performed using the free, open-access image analysis software QuPath (v3.0.0).(6) On the randomly selected images, the tumor areas were annotated manually based on the nuclear counterstain. For FAP quantification (positive area percentage) the intensity threshold was manually defined, and

settings were kept constant for all images and all different tumors. A macro script was written to allow automation of FAP quantification. FAP expression was correlated to the corresponding *ex vivo* radiotracer uptake in the tumor.

Measurement of FAP activity in tumor tissue. Tumor samples were snap-frozen in liquid nitrogen and crushed in a pre-cooled mortar on dry ice using liquid nitrogen to avoid loss of proteolytic activity due to temperature increase. Afterwards, the samples were lysed (1:10 sample weight : volume lysis buffer) in lysis buffer (50 mM Tris-HCl pH 8.3, 10 mM EDTA, 1% n-octyl-β-D- and 70 µg/mL aprotinin) for 1 hour on ice with frequent agitation. Next, samples were centrifuged at 12.000 x g for 10 minutes at 4°C. The tumor supernatant was collected and immediately used to perform FAP activity measurements and a Bradford quantification assay. FAP activity measurements were performed using our in-house developed assay using Z-Gly-Pro AMC as the fluorogenic substrate and **1** (UAMC1110) as specific FAP inhibitor.[7]

Briefly, in a 96-well plate (half-area, Greiner Bio-One), 5 µL tumor supernatant was pre-incubated for 15 min at 37 °C with 10 µL of FAP inhibitor or solvent control (250 nM UAMC-1110 or 0.0025 % (v:v) DMSO in FAP assay buffer consisting of 100 mM Tris-HCl pH 8.0, 300 mM NaF, 1 mM EDTA and 50 mM salicylic acid). Afterward, 35 µL pre-heated substrate solution (Z-Gly-Pro-AMC in FAP assay buffer, final concentration 266 µM; Bachem, Bübendorf, Switzerland, cat nr: 4002518) was added and fluorescence was measured kinetically for 30 minutes at 37 °C using the Tecan Infinite® M200 Pro (excitation wavelength 380 nm and emission wavelength 465 nm; Tecan, Männedorf, Switzerland). Fluorescence intensity was related to an AMC standard curve (0.3125 µM-10 µM) in an identical buffer. FAP enzymatic activity was normalized to the total protein content in the samples by a Bradford protein quantification assay.

Statistical analysis. Experimental data were expressed as mean ± standard deviation (SD). All statistical analysis were performed using Prism (version 9.5.1; GraphPad Software). Data were statistically analyzed by the one-way analysis of variance (ANOVA) followed by Bonferroni correction. Statistical significance between two data sets was evaluated by the unpaired two-tailed Student *t* test. For correlation analysis, the Pearson correlation coefficient was computed. Differences between the groups were considered statistically significant if the *P* value of was less than 0.05.

ASSOCIATED CONTENT

Supporting Information: Characterization data for key compound **35** ('cold' reference of compound **10)**; Detailed inhibition assay procedures; Biodistribution graphic of FAP radioligands in U-87MG xenografts; Molecular Formula Strings.

AUTHOR INFORMATION

Corresponding Authors

* P.V.V.: phone: +32 3265 27 08; e-mail: pieter.vanderveken@uantwerpen.be

*F. E.: phone: +32 3265 44 90; e-mail: filipe.elvas@uantwerpen.be

CONFLICT OF INTEREST

Compound **10** is also described in a patent application that we submitted (PCT/EP2023/064880).

ACKNOWLEDGEMENTS

Nicolò Filippi, Yentl Van Rymenant, Sergei Grintsevich and Joni De Loose are indebted to FWO-Vlaanderen for personal fellowships.

ABBREVIATIONS USED

ACN, acetonitrile; BW, body weight; Cl, clearance; DIPEA, diisopropylethylamine; DMF, dimethyl formamide; DPP, dipeptidyl peptidase; EtOAc, ethyl acetate; FAP, fibroblast activation protein alpha; IP, intraperitoneal; IV, intravenous, MeOH, methanol; PEG, polyethylene glycol; PET, positron Emission Tomography; p.i., post-injection; PK, pharmacokinetics; PREP, prolyl oligopeptidase; SAR, structure–activity relationship; TEA, trimethylamine; TFA, trifluoroacetic acid; THF, tetrahydrofuran; UPLC-MS, ultra-performance liquid chromatography-mass spectrometry.

REFERENCES

(1) Puré, E.; Blomberg, R. Pro-tumorigenic roles of fibroblast activation protein in cancer: back to the basics. *Oncogene* **2018**, *37*, *32,* 4343-4357. DOI: 10.1038/s41388-018-0275-3;

(2) Hamson, E.J.; Keane, F.M.; Tholen, S.; Schilling, O. Gorrell, M.D. Understanding fibroblast activation protein (FAP): substrates, activities, expression and targeting for cancer therapy. *Proteomics Clin Appl.* **2014**, *8*, *(5-6)*, 454-63. DOI: 10.1002/prca.201300095.

(3) Fitzgerald, A.A.; Weiner, L.M. The role of fibroblast activation protein in health and malignancy. *Cancer Metastasis Rev.* **2020**, 39, 3, 783-803. DOI: 10.1007/s10555-020-09909-3.

(4) Keane, F.M.; Yao, T.W.; Seelk, S.; Gall, M.G.; Chowdhury, S.; Poplawski, S.E.; Lai, J.H.; Li, Y.; Wu, W.; Farrell, P.; Vieira de Ribeiro, A.J.; Osborne, B.; Yu, D.M.; Seth, D.; Rahman, K.; Haber, P.; Topaloglu, A.K.; Wang, C.; Thomson, S.; Hennessy, A.; Prins, J.; Twigg, S.M.; McLennan, S.V.;

McCaughan, G.W.; Bachovchin W.W.; Gorrell, M.D. Quantitation of fibroblast activation protein (FAP)-specific protease activity in mouse, baboon and human fluids and organs. *FEBS Open Bio* **2013**, *4*, 43-54. DOI: https://10.1016/j.fob.2013.12.001.

(5) Simon, T.; Salhia, B. Cancer-associated fibroblast subpopulations with diverse and dynamic roles in the tumor microenvironment. *Mol. Cancer Res.* **2022**, *20*, *2*,183-192. DOI: 10.1158/1541-7786.

(6) Scott, A.M.; Wiseman, G.; Welt, S.; Adjei, A.; Lee, F.T.; Hopkins, W.; Divgi, C.R.; Hanson, L.H.; Mitchell, P.; Gansen, D.N.; Larson, S.M.; Ingle, J.N.; Hoffman, E.W.; Tanswell, P.; Ritter, G.; Cohen, L.S.; Bette, P.; Arvay, L.; Amelsberg, A.; Vlock, D.; Rettig, W.J.; Old, L.J. A Phase I dose-escalation study of sibrotuzumab in patients with advanced or metastatic fibroblast activation protein-positive cancer. *Clin. Cancer Res.* **2003**, *9*, *5*, 1639-1647.

(7) Jansen, K.; Heirbaut, L.; Verkerk, R.; Cheng, J.D.; Joossens, J.; Cos, P.; Maes, L.; Lambeir, A.M.; De Meester, I.; Augustyns, K.; Van der Veken, P. Extended structure-activity relationship and pharmacokinetic investigation of (4-quinolinoyl)glycyl-2-cyanopyrrolidine inhibitors of fibroblast activation protein (FAP). *J. Med. Chem.* **2014**, *57*, *7*, 3053-3074. DOI: 10.1021/jm500031w.

(8) Jansen, K.; Heirbaut, L.; Cheng, J.D.; Joossens, J.; Ryabtsova, O.; Cos, P.; Maes, L.; Lambeir, A.M.; De Meester, I.; Augustyns, K.; Van der Veken, P. Selective inhibitors of fibroblast activation protein (FAP) with a (4-quinolinoyl)-glycyl-2-cyanopyrrolidine scaffold. *ACS Med. Chem. Lett.* **2013**, *4*, *5*, 491-496. DOI: 10.1021/ml300410d.

(9) Lindner, T.; Loktev, A.; Altmann, A.; Giesel, F.; Kratochwil, C.; Debus, J.; Jäger, D.; Mier, W.; Haberkorn U. Development of quinoline-based theranostic ligands for the targeting of

fibroblast activation protein. *J. Nucl. Med.* **2018**, *59*, *9*, 1415-1422. DOI: 10.2967/jnumed.118.210443.

(10) Mori, Y.; Dendl, K.; Cardinale, J.; Kratochwil, C.; Giesel, F.L.; Haberkorn U. FAPI PET: Fibroblast activation protein inhibitor use in oncologic and nononcologic disease. *Radiology*, **2023**, *306*, 2:e220749. DOI: https://10.1148/radiol.220749.

(11) Gu, B.; Xu, X.; Zhang, J.; Ou, X.; Xia, Z.; Guan, Q.; Hu, S.; Yang, Z.; Song, S. The added value of ^{68}Ga-FAPI PET/CT in patients with head and neck cancer of unknown primary with ^{18}F-FDG-negative findings. *J Nucl Med.* **2022** *63*, *6*, 875-881. DOI: https://10.2967/jnumed.121.262790.

(12) Lindner, T.; Altmann, A.; Giesel, F.; Kratochwil, C.; Kleist, C.; Krämer, S.; Mier, W.; Cardinale, J.; Kauczor, H.U.; Jäger, D.; Debus, J.; Haberkorn, U. ^{18}F-labeled tracers targeting fibroblast activation protein. *EJNMMI Radiopharm Chem.* **2021,** 1, 26. DOI: 10.1186/s41181-021-00144-x

(13) Giesel, F.L.; Adeberg, S.; Syed, M.; Lindner, T.; Jiménez-Franco, L.D.; Mavriopoulou, E.; Staudinger, F.; Tonndorf-Martini, E.; Regnery, S.; Rieken, S.; El Shafie, R.; Röhrich, M.; Flechsig, P.; Kluge, A.; Altmann, A.; Debus, J.; Haberkorn, U.; Kratochwil, C. FAPI-74 PET/CT Using Either ^{18}F-AlF or Cold-Kit ^{68}Ga Labeling: Biodistribution, radiation dosimetry, and tumor delineation in lung cancer patients. *J. Nucl. Med.* **2021**, 201-207. DOI: 10.2967/jnumed.120.245084

(14) Hu, K.; Li, J.; Wang, L.; Huang, Y.; Li, L.; Ye, S.; Han, Y.; Huang, S.; Wu, H.; Su, J.; Tang, G.; Preclinical evaluation and pilot clinical study of [^{18}F]AlF-labeled FAPI-tracer for PET imaging of cancer associated fibroblasts. *Acta Pharm. Sin. B*. **2022**, 2, 867-875. doi: 10.1016/j.apsb.2021.09.032.

(15) Huang, J.; Fu, L.; Hu, K.; Huang, S.; Han, Y.; Lin, R.; Xu, W.; Tang, G.; Huang, Y. Automatic production and preliminary PET imaging of a new imaging agent [^{18}F]AlF-FAPT. *Front Oncol.* **2022**, 11, 802676. doi: 10.3389/fonc.2021.802676.

(16) See for example: (a) Rosenkrans, Z.T.; Massey, C.F.; Bernau, K.; Ferreira, C.A.; Jeffery, J.J.; Schulte, J.J.; Moore, M.; Valla, F.; Batterton, J.M.; Drake, C.R.; McMillan, A.B.; Sandbo, N.; Pirasteh, A.; Hernandez, R. [^{68}Ga]Ga-FAPI-46 PET for non-invasive detection of pulmonary fibrosis disease activity. *Eur. J. Nucl. Med. Mol. Imaging* **2022**, 49, 11, 3705-3716. DOI: 10.1007/s00259-022-05814-9.

(17) Scharitzer, M.; Macher-Beer, A.; Mang, T.; Unger, L.W.; Haug, A.; Reinisch, W.; Weber, M.; Nakuz, T.; Nics, L.; Hacker, M.; Bergmann, M.; Rasul, S. Evaluation of intestinal fibrosis with ^{68}Ga-FAPI PET/MR enterography in Crohn's disease. *Radiology* **2023**, *307*, 3:e222389. DOI: https://10.1148/radiol.222389.

(18) Toms, J.; Kogler, J.; Maschauer, S.; Daniel, C.; Schmidkonz, C.; Kuwert, T.; Prante, O. Targeting fibroblast activation protein: radiosynthesis and preclinical evaluation of an ^{18}F-labeled FAP inhibitor. *J Nucl Med.* **2020**, 12, 1806-1813. DOI: https://10.2967/jnumed.120.242958.

(19) Poulie, C.B.M.; Shalgunov, V.; Elvas, F.; Van Rymenant, Y.; Moon, E.S.; Battisti, U.M.; De Loose, J.; De Meester, I.; Rösch, F.; Van Der Veken, P.; Herth, M.M. Next generation fibroblast activation protein (FAP) targeting PET tracers - The tetrazine ligation allows an easy and convenient way to ^{18}F-labeled (4-quinolinoyl)glycyl-2-cyanopyrrolidines. *Eur. J. Med. Chem.* **2023,** 262,115862. DOI: https://10.1016/j.ejmech.2023.115862.

(20) Zhang, M.R.; Maeda, J.; Ito, T.; Okauchi, T.; Ogawa, M.; Noguchi, J.; Suhara, T.; Halldin, C.; Suzuki K. Synthesis and evaluation of *N*-(5-fluoro-2-phenoxyphenyl)-*N*-(2-

[^{18}F]fluoromethoxy-d_2-5-methoxybenzyl)acetamide: a deuterium-substituted radioligand for peripheral benzodiazepine receptor. *Bioorg. Med. Chem.* **2005**, *13*, *5*,1811-1818. DOI: 10.1016/j.bmc.2004.11.058.

(21) Nemoto, H.; Cai, J.; Asao, N.; Iwamoto, S.; Yamamoto, Y. Synthesis and biological properties of water-soluble *p*-boronophenylalanine derivatives. Relationship between water solubility, cytotoxicity, and cellular uptake. *J. Med. Chem.* **1995**, 38, 10, 1673-1678. DOI: 10.1021/jm00010a012

(22) Oh, S.J.; Chi, D.Y.; Mosdzianowski, C.; Kim, J.Y.; Gil, H.S.; Kang, S.H.; Ryu, J.S.; Moon, D.H. Fully automated synthesis of [^{18}F]fluoromisonidazole using a conventional [^{18}F]FDG module. *Nucl. Med. Biol.* **2005**, 32, 8, 899-905. DOI: 10.1016/j.nucmedbio.2005.06.003

(23) Van Rymenant, Y.; Tanc, M.; Van Elzen, R.; Bracke, A.; De Wever, O.; Augustyns, K.; Lambeir, A.M.; Kockx, M.; De Meester, I.; Van Der Veken, P. *In vitro* and *in situ* activity-based labeling of fibroblast activation protein with UAMC1110-derived probes. *Front. Chem.* **2021**, *14*, 9:640566. DOI: 10.3389/fchem.2021.640566.

(24) Beyerlein, F.; Piel, M.; Höhnemann, S.; Rösch, F. Automated synthesis and purification of [^{18}F]fluoro-[di-deutero]methyl tosylate. *J. Labelled Comp. Radiopharm.* **2013**, *56*, *7*, 360-363. DOI: 10.1002/jlcr.3043.

(25) Xu, Y.; Mu, J.; Xu, Z.; Zhong, H.; Chen, Z.; Ni, Q.; Liang, X.J.; Guo, S. Modular acid-activatable acetone-based ketal-linked nanomedicine by dexamethasone prodrugs for enhanced anti-rheumatoid arthritis with low side effects. *Nano Lett.* **2020**, 20, (4):2558-2568. DOI: 10.1021/acs.nanolett.9b05340

(26) Moon, E.S.; Elvas, F.; Vliegen, G.; De Lombaerde, S.; Vangestel, C.; De Bruycker, S.; Bracke, A.; Eppard, E.; Greifenstein, L.; Klasen, B.; Kramer, V.; Staelens, S.; De Meester, I.; Van der Veken, P.; Rösch F. Targeting fibroblast activation protein (FAP): next generation PET radiotracers using squaramide coupled bifunctional DOTA and DATA^{5m} chelators. *EJNMMI Radiopharm Chem.* **2020**, *5*, *1*, 19. DOI: 10.1186/s41181-020-00102-z

(27) Greifenstein, L.; Kramer, C.S.; Moon, E.S.; Rösch, F.; Klega, A.; Landvogt, C.; Müller, C.; Baum, R.P. From Automated Synthesis to In Vivo Application in Multiple Types of Cancer-Clinical Results with [^{68}Ga]Ga-DATA^{5m}.SA.FAPi. *Pharmaceuticals* **2022,** *15*, *8*,1000. DOI: 10.3390/ph15081000

(28) Breznik, B.; Motaln, H.; Vittori, M.; Rotter, A.; Lah Turnšek, T. Mesenchymal stem cells differentially affect the invasion of distinct glioblastoma cell lines. *Oncotarget* **2017**, *8*, *15*, 25482-25499. DOI: 10.18632/oncotarget.16041.

(29) Tran, E.; Chinnasamy, D.; Yu, Z.; Morgan, R.A.; Lee, C.C.; Restifo, N.P.; Rosenberg, S.A. Immune targeting of fibroblast activation protein triggers recognition of multipotent bone marrow stromal cells and cachexia. *J. Exp. Med.* **2013**, *210*, *6*, 1125-1135. DOI: 10.1084/jem.20130110.

(30) Wei, H.; Xu, Y.; Wang, Y.; Xu, L.; Mo, C.; Li, L.; Shen, B.; Sun, Y.; Cheng, P.; Yang, L.; Pang, Y.; Qin, A.; Cao, Y.; Morrison, S.J.; Yue, R. Identification of Fibroblast Activation Protein as an Osteogenic Suppressor and Anti-osteoporosis *Drug Target. Cell Rep.* **2020**, *33*, *2*, 108252. DOI: 10.1016/j.celrep.2020.108252.

(31) Hamada, H.; Kobune, M.; Nakamura, K.; Kawano, Y.; Kato, K.; Honmou, O.; Houkin, K.; Matsunaga, T.; Niitsu, Y. Mesenchymal stem cells (MSC) as therapeutic cytoreagents for gene therapy. *Cancer Sci.* **2005**, *96*, *3*,149-56. DOI: 10.1111/j.1349-7006.2005.00032.x

(32) Kaplan, R.N.; Psaila, B.; Lyden, D. Niche-to-niche migration of bone-marrow-derived cells. *Trends Mol. Med.* **2007**, *13*, *2*, 72-81. DOI: 10.1016/j.molmed.2006.12.003

(33) Wen, X.; Xu, P.; Shi, M.; Liu, J.; Zeng, X.; Zhang, Y.; Shi, C.; Li, J.; Guo, Z.; Zhang, X.; Khong, P.L.; Chen X. Evans blue-modified radiolabeled fibroblast activation protein inhibitor as long-acting cancer therapeutics. *Theranostics* **2022**, *12, 1*, 422-433. DOI: 10.7150/thno.68182.

(34) Lindeman, S.D.; Mukkamala, R.; Horner, A.; Tudi, P.; Booth, O.C.; Huff, R.; Hinsey, J.; Hovstadius, A.; Martone, P.; Zhang, F.; Srinivasarao, M.; Cox, A.; Low, P.S. Fibroblast activation protein-targeted radioligand therapy for treatment of solid tumors. *J. Nucl. Med.* **2023**, *64*, 5:759-766. DOI: 10.2967/jnumed.122.264494.

(35) Benramdane, S.; De Loose, J.; Beyens, O.; Van Rymenant, Y.; Vliegen, G.; Augustyns, K.; De Winter, H.; De Meester, I.; Van der Veken, P. Vildagliptin-derived dipeptidyl peptidase 9 (DPP9) inhibitors: identification of a DPP8/9-specific lead. *ChemMedChem* **2022**, 17, (15), e202200097. DOI: 10.1002/cmdc.202200097

(36) De Meester, I.; Vanhoof, G.; Lambeir, A.-M.; Scharpé, S. Use of immobilized adenosine deaminase (EC 3.5.4.4) for the rapid purification of native human CD26/dipeptidyl peptidase IV (EC 3.4.14.5). *J. Immunol. Methods* **1996**, *189* (1), 99-105. DOI: 10.1016/0022-1759(95)00239-1

(37) De Decker, A.; Vliegen, G.; Van Rompaey, D.; Peeraer, A.; Bracke, A.; Verckist, L.; Jansen, K.; Geiss-Friedlander, R.; Augustyns, K.; De Winter, H.; De Meester, I.; Lambeir, A.M.; Van der Veken P. Novel small molecule-derived, highly selective substrates for fibroblast activation protein (FAP). *ACS Med. Chem. Lett.* **2019**, *10* (8), 1173-1179. DOI: 10.1021/acsmedchemlett.9b00191

TOC GRAPHIC